HHS Public Access

Author manuscript

Dev Dyn. Author manuscript; available in PMC 2024 May 01.

Published in final edited form as:

Dev Dyn. 2023 May ; 252(5): 605–628. doi:10.1002/dvdy.566.

Functional comparison of human ACVR1 and zebrafish Acvr1l FOP-associated variants in embryonic zebrafish

Robert L. Lalonde[1], **Hannah A. Nicolas**[2], **Rowan S. Cutler**[1], **Irene Pantekidis**[1], **Weibo Zhang**[1], **Pamela C. Yelick**[1,*]

[1]Tufts University School of Dental Medicine, Division of Craniofacial and Molecular Genetics, 136 Harrison Avenue, Boston, MA, USA 02111

[2]Department of Biology, Faculty of Science, University of Ottawa, Ottawa, ON, Canada K1N 6N5

Abstract

Background: Fibrodysplasia ossificans progressiva (FOP), a rare disease characterized by progressive heterotopic ossification of muscle and connective tissues, is caused by autosomal dominant activating mutations in the type I receptor, ACVR1/ALK2. The classic human FOP variant, ACVR1^{R206H}, shows increased BMP signaling and activation by Activins.

Results: Here we performed *in vivo* functional characterization of human ACVR1^{R206H} and orthologous zebrafish Acvr1l^{R203H} using early embryonic zebrafish dorsoventral patterning as a phenotypic readout for receptor activity. Our results showed that human ACVR1^{R206H} and zebrafish Acvr1l^{R203H} exhibit functional differences in early embryonic zebrafish, and that human ACVR1^{R206H} retained its signaling activity in the absence of a ligand-binding domain (LBD). We also showed, for the first time, that zebrafish Acvr2ba/Acvr2bb receptors are required for human ACVR1^{R206H} signaling in early embryonic zebrafish.

Conclusions: Together, these data provide new insight into ACVR1^{R206H} signaling pathways that may facilitate the design of new and effective therapies for FOP patients.

Introduction

Fibrodysplasia ossificans progressiva (FOP) is a rare autosomal dominant disease characterized by the progressive onset of heterotopic ossification (HO) in muscle and connective tissue [1–4]. While early stage FOP patients exhibit increasingly limited mobility, as the disease progresses patients form excessive HO that eventually results in death due to thoracic insufficiency [5,6]. HO can also be exacerbated by injury, hampering FOP patient treatment [1,2(p2),3,4]. It was previously shown that heterozygous mutations in the type I TGFβ family receptor ACVR1 (Activin A receptor Type I/ ALK2) are causative for FOP [3,7,8]. Consistent with other type I TGFβ family member receptors, ACVR1 is composed of a ligand-binding domain (LBD), a transmembrane domain (TMD), a GS-rich domain, and a

*Corresponding author Pamela.Yelick@tufts.edu.

Author Contributions

R. L. L. performed all experimentation except for western blots analysis and wrote the manuscript. R. L. L. and P. C. Y. conceptualized the project. R.S.C, W.Z. and P.C.Y. performed western blot analysis. I. P. propagated the transgenic and mutant lines. R. L. L., H.A.N and P. C. Y. analyzed the data. P. C. Y. supervised the project, secured funding, and revised the manuscript.

protein kinase domain (KD) [9–12]. Upon binding BMP5/7 heterodimer or Activin A dimer ligands, ACVR1/Type I receptor heterodimers can oligomerize with a variety of type II receptor dimers including ACVR2A, ACVR2B and BMPR2, leading to ACVR1 activation by phosphorylation in the GS domain, rendering it competent to phosphorylate downstream SMAD1/5/8 signaling partners [9–14], which translocate to the nucleus and induce gene expression. Type I receptor phosphorylation by type II receptors induce conformational changes leading to the disassociation of FKBP12/FKBP1A, which normally safeguard against leaky BMP signaling [15–18].

Approximately 97% of FOP patients have the classic *ACVR1*^{R206H} mutation located in the GS-rich domain [3,7,9,19,20]. FOP associated ACVR1 mutations can also occur in the kinase domain, which normally directs phosphorylation of downstream SMADs1/5/8 [7,21,22]. Previous *in vitro* studies showed that ACVR1^{R206H} exhibits increased responsiveness to BMP ligands including BMP2, BMP4, BMP7, BMP9, and BMP10 [23–25]. In addition, although wildtype (WT) ACVR1 is normally inhibited by Activin in some cell types, which blocks BMP signaling through type II receptors ACVR2A and ACVR2B [14,26–28], the FOP variant ACVR1^{R206H} is activated by Activins to signal through BMP signaling SMADs [9,23,29]. A proposed mechanism for increased activity of ACVR1^{R206H} is reduced binding affinity for the inhibitors FKBP12/FKBP1A [15,17,30].

BMP signaling contributes to early embryonic patterning and adult tissue formation, including endochondral and intramembranous bone formation [12,31–34]. BMP signaling in early embryonic zebrafish dorsoventral patterning has been extensively studied using a variety of zebrafish mutants [34–42]. Zebrafish mutants with upregulated BMP signaling, such as *chordino*, which harbors a mutation in the BMP-antagonist *chordin,* display ventralization phenotypes, scored as V1-V5 based on severity [34,38,39,43,44]. In contrast, mutants with decreased BMP signaling, such as *Snailhouse/bmp7*, *Twist/bmp2b* and *somitabun*/*smad5*, exhibit dorsalized phenotypes, scored C1-C5 based on severity [37,45,46]. The zebrafish *acvr1l*/*alk8* mutant, "*lost-a-fin"* (the zebrafish ortholog to human *ACVR1/ALK2*), displays an early lethal C2-dorsalization phenotype largely restricted to the ventral tail fin and heart [38,47]. Single cell stage injection of dominant-negative *acvr1l* mRNA induces a spectrum of dorsalization phenotypes (C1-C5), while constitutively-active *acvr1l*^{Q204D} mRNA induces a spectrum of ventralization phenotypes (V1-V5) [38,47,48]. Heat-shock inducible transgenic zebrafish expressing *acvr1l*^{Q204D} beginning at 4 hours post-fertilization (hpf) also ventralize (V3) and exhibit increased pSmad1/5 activity [49] using *in vivo* reporter BMP response element (BRE):GFP transgenic zebrafish [50,51].

Based on the extensive body of published reports characterizing BMP signaling in early embryonic zebrafish dorsoventral patterning, embryonic zebrafish have become a useful tool for investigating FOP-associated *ACVR1* variant activity. The fact that WT human (*Homo sapiens, Hs*) *ACVR1* mRNA can rescue zebrafish (*Danio rerio, Dr*) *acvr1l/laf* mutants suggests that human *ACVR1* and zebrafish *acvr1l* are functionally conserved [30]. Injection of FOP variant *Hs-ACVR1*^{R206H} mRNA into single cell stage zebrafish induces a spectrum of ventralization phenotypes and increased phosphorylated-Smad1/5 (pSmad1/5) levels in embryonic zebrafish [30]. Kinase domain FOP-associated ACVR1 variants including ACVR1 Gly328 to Trp, Glu, or Arg also induce ventralization and increased pSmad1/5 in embryonic

zebrafish [22]. These results support *in vitro* studies showing increased BMP-signaling activity of these FOP-associated *Hs-ACVR1* variants. To date, no one has determined whether orthologous zebrafish *Dr-acvr1l*^{R203H} also exhibits increased BMP-signaling activity. Our studies here exploit embryonic zebrafish models to expand our knowledge of human ACVR1^{R206H} signaling mechanisms, and also those of zebrafish Acvr1l^{R203H}.

Here we used the zebrafish embryo as an *in vivo* model to define the functional domains and type II receptor signaling partners of FOP-associated human Hs-ACVR1^{R206H} and orthologous zebrafish Dr-Acvr1l^{R203H,} taking advantage of the well-established embryonic dorsalization (C1-C5) and ventralization (V1-V5) phenotypes as a read-out for global Bmp signaling[30,37,52–54]. Using heat-shock (HS) inducible transgenic lines, mRNA injections, anti-sense morpholino oligomer (MO) injections, and CRISPR/Cas9 Homology Directed Repair (HDR) approaches, we showed that *Hs-ACVR1*^{R206H} and *Dr-acvr1l*^{R203H} exhibit functional differences in embryonic zebrafish. While *Dr-acvr1l*^{R203H} exhibits WT *Dr-acvr1l* functions in early embryonic zebrafish, in contrast, *Hs-ACVR1*^{R206H} induced ventralized embryonic phenotypes consistent with upregulated BMP signaling. Using chimeric human/zebrafish *ACVR1/acvr1l* and ligand binding domain (LBD) deletion expression constructs, we demonstrated that this functional diversity is mediated by the ACVR1^{R206H} GS-rich and/or kinase domains, and that ACVR1^{R206H} signaling is maintained without its LBD in the zebrafish embryo. We also show that WT Hs-ACVR1 and Dr-Acvr1l require their respective LBDs for proper function. Finally, using previously published type II TGFβ family member receptor anti-sense morpholinos (MOs)[55,56] in combination with our heat-shock inducible *Hs-ACVR1*^{R206H} transgenic zebrafish, we demonstrated that zebrafish Acvr2ba/Acvr2bb, and not Acvr2aa/Acvr2ab, are required for Hs-ACVR1^{R206H} activity, indicating that Acvr2b paralogs are the type II signaling partners for Hs-ACVR1^{R206H} in early embryonic zebrafish.

Results

Zebrafish *acvr1l*^{R203H} and human *ACVR1*^{R206H} show functional differences in early embryonic zebrafish.

Characterizing HS-inducible transgenic zebrafish lines.—To model human FOP in zebrafish, we created heat-shock (HS) inducible transgenic lines expressing: WT zebrafish *acvr1l (Dr-acvr1l)*; the human *ACVR1*^{R206H} FOP variant (*Hs-ACVR1*^{R206H}); and the orthologous zebrafish variant *acvr1l*^{R203H} (*Dr-acvr1l*^{R203H}). The Hs-ACVR1^{R206H} and the Dr-acvr1l^{R203H} mutations are located with the GS-rich domain (Fig. 1A) and each coding region was fused to an *mCherry* reporter gene. These transgenic lines will henceforth be known as *Tg(Dr-acvr1l-WTa), Tg(Hs-R206Ha),* and *Tg(Dr-R203Ha)*, respectively. We previously showed that heat-shock (HS) was an effective strategy to express the constitutively-active *Dr-acvr1l*^{Q204D} variant in embryonic and adult zebrafish [49,57,58]. Consistent with the fact that Hs-ACVR1^{R206H} signals through pSMAD1/5/8 [59], it was previously shown that injection of *Hs-ACVR1*^{R206H} mRNA into single cell stage zebrafish resulted in increased pSmad1/5 expression and ventralization phenotypes [30]. Characterization of zebrafish *Dr-acvr1l*^{R203H} expression has not been reported to date.

To compare the activities of heat-shock inducible mCherry-tagged *Hs-ACVR1(WT), Hs-ACVR1^{R206H}*, *Dr-acvr1l^{R203H}* and *Dr-acvr1l(WT)*, we performed one hour HS on clutches of transgenic embryos at 4hpf and screened them for dorsoventral phenotypes at 24hpf. *HS-Tg(Dr-acvr1l-WTa)* zebrafish exhibited *mCherry* expression but no dorsoventral phenotypes (Fig. 2A–B). In contrast, *HS-Tg(Hs-R206Ha)* zebrafish showed severe ventralization (V5) phenotypes (Fig. 2C–D). This ventralization phenotype is consistent with *bmp2b* and *bmp4* overexpression phenotypes that produced “spindle-shaped” embryos and is consistently more severe than Bmp antagonist mutants [53,60]. Surprisingly, *HS-Tg(Dr-R203Ha)* zebrafish did not exhibit any ventralized phenotypes despite strong *mCherry* expression following 1 or 2 hour heat-shock treatment (Fig 2E–F, L). These results, which were confirmed using independently generated founders [*Tg(Dr-acvr1l-WTa, b)*, *Tg(Dr-R203Ha, b, c)* and *Tg(Hs-R206Ha, b, c)*], suggested that *Dr-acvr1l^{R203H}* and *Hs-ACVR1^{R206H}* exhibit functional differences in embryonic zebrafish. Multiple clutches from each founder were analyzed, and the described phenotypes were 100% penetrant in F1 zebrafish for all transgenic lines.

To account for transgene variability in each transgenic line, we performed CTCF (Corrected Total Cell Fluorescence) calculations in F1s from individual founder zebrafish. Using CTCF analysis, we documented that decreased *Tg(Hs-R206H)* expression (down to 0.25x fluorescence intensity), still resulted in V5-ventralization phenotypes (Fig. 2K), and that increased *Tg(Dr-R203H)* expression (up to ~3x fluorescence intensity) resulted in normal embryonic development (Fig. 2L). We also show that two hour heat-shock of *Tg(Dr-R203Ha)* F1s increased the fluorescent intensity by ~1.6x in some F1 embryos, while not affecting development (Fig. 2L). It should be noted that HS *Tg(Hs-R206H)* and *Tg(Dr-R203H)* transgenic lines could not be directly compared due to severely ventralized phenotype of *HS-R206H* embryos.

To directly compare mCherry-tagged protein levels between HS-*Tg(Dr-acvr1l-WTa)*, HS-*Tg(Hs-R206H)* and Hs-*Tg(Dr-R203H),* we performed Western Blot analysis. At 5dpf, embryos were heat-shocked for one hour, and protein extractions were performed 6 hours later. Under these conditions, *Tg(Dr-acvr1l-WTa)* embryos displayed significantly higher levels of mCherry as compared to both mutant variant line embryos, and no significant difference was observed between HS-*Tg(Hs-R206H)* and Hs-*Tg(Dr-R203H)* (Fig. 2M–N). Together these results support that the lack of phenotype in *Tg(Dr-acvr1l-WTa)* and Hs-*Tg(Dr-R203H)* embryos is not due to reduced transgene expression.

To correlate observed phenotypes with pSmad1/5 signaling, as supported by previously published experimental data[30], we performed Western Blot analysis for pSmad1/5 expression in HS 5dpf zebrafish embryos (Fig. 2N–O). We chose to conduct HS at 5 hpf due to the severe ventralization phenotypes of 24 hpf HS-*Tg(Hs-R206H)* following 4hpf heat-shock, which prevented us from obtaining sufficient amounts of protein for repeated western blot analysis. Under these conditions, HS-*Tg(Hs-R206H)* embryos did not show significantly higher pSmad1/5 levels compared to *Tg(Dr-acvr1l-WTa)* and Hs-*Tg(Dr-R203H),* although p-value trended towards significance (p=0.1657, p=0.1383) (Fig. 2N–O). We next correlated pSmad1/5 expression with mCherry tagged protein expression (Fig. 2M–P), which demonstrated significantly higher levels of pSmad1/5 relative to mCherry expression in HS *Tg(Hs-R206H*) embryos as compared to both *Tg(Dr-acvr1l-WTa)*

(p=0.0084) and Hs-*Tg(Dr-R203H)* (p=0.0187) (Fig. 2P). Together, these results demonstrate increased pSmad1/5 signaling in HS *Tg(Hs-R206H)* zebrafish as compared to heat-shocked *Tg(Dr-acvr1l-WTa)* and Hs-*Tg(Dr-R203H)* embryos.

Validation of Hs-ACVR1/Dr-Acvr1l WT and FOP variants using mRNA injection approaches.

To confirm the results obtained using our HS inducible transgenic zebrafish lines, here we injected *Hs-ACVR1(WT), Dr-acvr1l(WT), Hs-ACVR1*^{R206H}, or *Dr-acvr1l*^{R203H} mRNAs into single cell stage zebrafish embryos and assessed phenotypes at 24hpf. No altered phenotypes were observed following injection of WT *Dr-acvr1l* or WT *Hs-ACVR1* mRNAs at two different concentrations (Fig. 2G, 6J). In contrast, and as previously shown [30], injection of *Hs-ACVR1*^{R206H} mRNA induced a spectrum of ventralization phenotypes (V1-V5) (Fig. 2H–I, Q, Columns 3–4). As previously described, this spectrum consisted of a progressive loss of anterior features including eyes, head and notochord, an expansion of posterior somites, and enlarged blood islands (Kishimoto et al. 1997). V5 embryos lacked all anterior structures. Injection of *Dr-acvr1l*^{R203H} mRNA at equal or two fold concentrations did not result in any ventralization phenotypes, consistent with our transgenic *HS-Tg(Dr-R203Ha, b, c)* line results (Fig. 2J, Q, Columns 1–2). Together, these results validate results obtained using our HS inducible transgenic lines and indicate that *Dr-acvr1l*^{R203H} does not exhibit upregulated BMP signaling as compared to *Hs-ACVR1*^{R206H} in embryonic zebrafish. While this result was unexpected, it provided an opportunity to identify the functional domains that differ between the human and zebrafish variants, and those that are required for Hs-ACVR1^{R206H} signaling.

Zebrafish *acvr1l*$^{\Delta 13bp/\Delta 13bp}$ homozygous mutants can be rescued by WT zebrafish *acvr1l* and WT human *ACVR1* mRNAs.

To perform functional analyses of WT *Dr-acvr1l* and WT *Hs-ACVR1,* we tested whether they each could rescue homozygous *acvr1l* loss-of-function zebrafish mutants. First, as described in Methods, we created an *acvr1l* allele containing a 13bp deletion (Δ13bp) that removes an HhaI restriction site, facilitating genotyping of WT (cut) and edited (uncut) zebrafish (Fig. 3A–B, M). The deletion leads to a frameshift in the GS domain starting at Valine 201, that results in a premature stop codon at amino acid 224 (Fig. 1A, Fig. 3A–B). Homozygous *acvr1l*$^{\Delta 13bp/\Delta 13bp}$ zebrafish exhibit a fully penetrant C2-dorsalization phenotype indistinguishable from that of the previously characterized *acvr1l/laf*^{m100}and *laf*^{tm110} mutants [38,47] (Fig. 3C–D). As with *laf* mutants, 1 dpf *acvr1l*$^{\Delta 13bp/\Delta 13bp}$ embryos lack their ventral tail fin and vein and die by ~3dpf (Mintzer et al. 2001). Complementation analysis and genomic sequencing was used to validate the *acvr1l*$^{\Delta 13bp}$ allele (Fig. 3E). RT-PCR, and subsequent sequencing of *acvr1l*$^{\Delta 13bp}$ transcript revealed no evidence of exon-skipping (Fig. 3F). At 28hpf, *acvr1l*$^{\Delta 13bp/\Delta 13bp}$ embryos showed a slight decrease in transcript levels as compared to WT (Fig. 3F). We next showed that the C2-dorsalization *acvr1l*$^{\Delta 13bp/\Delta 13bp}$ embryonic phenotype could be rescued by single cell injection of WT *Dr-acvr1l* or *Hs-ACVR1* mRNA (Fig. 3G–L). WT *Dr-acvr1l* mRNA injection into *acvr1l*$^{\Delta 13bp/+}$ incrossed progeny resulted in no C2-dorsalization phenotypes (0%), and only a small number of mild C1-dorsalization phenotypes (3.6%, partial rescue) (Fig. 3G–H, L). Compared to C2-dorsalization, C1-dorsalized embryos display a milder ventral fin defect where the ventral tail vein forms, and these embryos

generally survive (Kishimoto et al. 1997). Similarly, injection of WT *Hs-ACVR1* mRNA into *acvr1l*$^{\Delta 13bp/+}$ incrossed progeny resulted in only a small number of C2 (6.94%, no rescue) and C1-dorsalization phenotypes (5.55%, partial rescue) (Fig. 3I–L). The progeny of uninjected *acvr1l*$^{\Delta 13bp/+}$ adult incrossed progeny consistently yielded ~25% C2-dorsalized embryos, similar to that of previously published *acvr1l* homozygous mutants (Fig. 3L). To more conclusively show that *Hs-ACVR1* can rescue C2-dorsalization of homozygous *acvr1l*$^{\Delta 13bp/\Delta 13bp}$ mutant zebrafish, we genotyped 13 individual injected embryos with WT phenotypes and identified 5 fully rescued homozygous *acvr1l*$^{\Delta 13bp/\Delta 13bp}$ zebrafish (Fig. 3M–N). Although not statistically significant, the presence of partially rescued C1 embryos and phenotypically normal *acvr1l*$^{\Delta 13bp/\Delta 13bp}$ homozygous mutants confirms that Hs-ACVR1 can rescue *acvr1l* homozygous zebrafish mutants. These results suggest that WT *Hs-ACVR1* and WT *Dr-acvr1l* are functionally conserved in early embryonic zebrafish, and that both can rescue the homozygous *acvr1l*$^{\Delta 13bp}$ loss-of-function mutation.

The zebrafish Dr-Acvr1l^{R203H} variant can rescue WT Dr-Acvr1l function in early embryonic zebrafish.

To further evaluate Dr-acvr1l^{R203H} function in early embryonic zebrafish, we created an endogenous zebrafish *acvr1l*^{R203H} allele using a CRISPR/cas9 homology directed repair (HDR) approach (see Methods). The resulting R203H amino acid substitution destroys an HhaI restriction site that was used to facilitate genotyping (Fig. 4A–B; Fig. 3M). This targeted editing also inadvertently introduced an additional silent SNP 6bp upstream (A>G), which did not result in an amino acid change (Fig. 4A–B). Homozygous zygotic *acvr1l*$^{R203H/R203H}$ (n = 500–1000, 3 clutches) and maternal/zygotic *acvr1l*$^{R203H/R203H}$ embryos showed no phenotype (n = 1000–1500, 4 clutches) (Fig. 4C–F), suggesting that the *Dr-Acvr1l*^{R203H} allele functions normally in place of WT *Dr-acvr1l* in the early zebrafish embryo. At 5 dpf, *acvr1l*$^{R203H/R203H}$ zebrafish show no significant difference in pSmad1/5 levels compared to *HS-Tg(Dr-acvr1l-WTa)*, *HS-Tg(Dr-R203Ha),* and *HS-Tg(Hs-R206Ha)* as measured by western blot analysis. pSmad1/5 levels in *HS-Tg(Hs-R206Ha)* compared to *acvr1l*$^{R203H/R203H}$ trends towards significance (p=0.1593) (Fig. 2N–O). Nine homozygous maternal/zygotic (MZ) *acvr1l*$^{R203H/R203H}$ zebrafish embryos with WT phenotypes were genotyped to confirm (Fig. 4J). Using a complementary approach, progeny from crossed *Tg(Dr-R203Ha)* and heterozygous *acvr1l*$^{\Delta 13bp/+}$ zebrafish mutants were raised to adulthood (Fig. 4G–I), to create *Dr-acvr1l*$^{\Delta 13bp/+}$ adults in the *Tg(Dr-R203Ha)* background. These adults were incrossed, and a proportion of their progeny were HS at 4hpf. The non-HS siblings showed C2-dorsalization phenotypes at 24hpf (*acvr1l*$^{\Delta 13bp/\Delta 13bp}$ mutants, 17.2% n = 5/29) (Fig. 4G). Within the 50 heat-shocked HS-*Tg(Dr-R203Ha)* siblings, 10/50 showed faint *mCherry* expression, of which roughly a quarter (n = 3/10) exhibited C2-dorsalization phenotypes (Fig. 4H). This suggests that low levels of *Dr-acvr1l*^{R203H} mRNA cannot rescue *Dr-acvr1l*$^{\Delta 13bp/\Delta 13bp}$ mutants. However and in contrast, all of the heat-shocked HS-*Tg(Dr-R203Ha)* siblings with bright *mCherry* expression (n=40/50) showed a WT phenotype (Fig. 4I), suggesting that strong expression of *Dr-acvr1l*^{R203H} mRNA can rescue *Dr-acvr1l*$^{\Delta 13bp/\Delta 13bp}$ mutants. To conclusively demonstrate that high levels of *Tg(Dr-R203Ha)* expression can rescue C2-dorsalization in homozygous *acvr1l*$^{\Delta 13bp/\Delta 13bp}$ zebrafish, we genotyped 14 WT looking embryos with bright *mCherry* expression and identified 5 homozygous *acvr1l*$^{\Delta 13bp/\Delta 13bp}$ zebrafish (Fig. 4K). Together, these results

indicated that the *Dr-acvr1l*^{R203H} allele exhibits WT Dr-Acvr1l function in early embryonic zebrafish, supporting our *Dr-acvr1l*^{R203H} mRNA injection and transgenic heat-shock assay data.

The human ACVR1^{R206H} GS-rich and Kinase domains direct ventralization of early embryonic zebrafish.

"To further investigate the observed signaling difference between Dr-Acvr1l^{R203H} and Hs-ACVR1^{R206H}, we performed an amino acid sequence comparison to identify differences in key functional domains of the two receptor variants (Fig. 1A)[9,20]. While the GS and KD amino acid sequences are well conserved between these two proteins (86.16% amino acid sequence identity), the N-termini containing the LBD and TMD are less conserved (29.59% amino acid sequence identity) (Fig. 1A). We therefore wondered whether the N-terminal or C-terminal sequences regulated receptor function in early embryonic zebrafish. To test this, we created chimeric expression constructs consisting of the zebrafish Dr-Acvr1l^{R203H} N-terminus fused to the human ACVR1^{R206H} C-terminal amino acids, and vice-versa. These constructs were termed: *Dr-ECD-TMD + Hs-GS-KD* (***D****anio* ***r****erio* **E**xtra**C**ellular **D**omain – **T**rans**M**embrane **D**omain + ***H****omo* ***s****apien* **GS**-rich domain-**K**inase **D**omain) and *Hs-ECD-TMD + Dr-GS-KD* (***H****omo* ***s****apien* **E**xtra**C**ellular **D**omain – **T**rans**M**embrane **D**omain + ***D****anio* ***r****erio* **GS**-rich domain-**K**inase **D**omain). The domains were fused at a location between the TMD and the GS, at position AA167 in Hs-ACVR1, and AA164 in Dr-Acvr1l. Due to the cloning strategy, both constructs contain an aspartic acid (D) at position AA167/AA164, respectively, similar to the negatively charged glutamic acid (E) present in the WT Hs-ACVR1 (Fig. 1A, 5A–E). Surprisingly, we found that single cell injection of *Dr-ECD-TMD + Hs-GS-KD* mRNA induced embryonic ventralization phenotypes (V1-V5) at 24hpf (Fig. 5B, D), suggesting that the Hs-ACVR1^{R206H} C-terminus was directing embryonic ventralization. In contrast, single cell injection of two different concentrations *Hs-ECD-TMD + Dr-GS-KD* mRNA yielded no phenotype, similar to the results obtained by single cell injections of *Dr-acvr1l*^{R203H} mRNA (Fig. 5C–D). Together with our previous results showing that Dr-Acvr1l^{R203H} exhibits WT Dr-Acvr1l signaling, our chimeric construct data suggest that amino acid differences between the Hs-ACVR1^{R206H} and Dr-Acvr1l^{R203H} GS rich and kinase domains play important roles in regulating the activities of these variant receptors.

The human ACVR1^{R206H} ligand-binding domain is not required for early embryonic zebrafish ventralized phenotype.

Previous *in vitro* studies showed that removal of the LBD of Hs-ACVR1^{R206H} resulted in a statistically significant decrease in the activity of Hs-ACVR1^{R206H}, as measured through relative *BRE:luciferase* activity [9,20,24]. We therefore sought to confirm these results in our *in vivo* embryonic zebrafish model, as compared to WT Dr-Acvr1l and Dr-Acvr1l^{R203H}. First, we removed the LBD of both the Hs-ACVR1 and Dr-Acvr1l proteins (Fig. 1A, highlighted in yellow), without introducing any other amino acid changes. Nucleotide sequence analyses were used to verify that all of the resulting LBD lacking WT and variant human and zebrafish ACVR1/Acvr1l constructs contained the exact same deletion, and no additional amino acid sequence differences. Next, we injected WT *Dr-acvr1l or WT Hs-ACVR1* mRNA lacking the LBD (*Dr-acvr1lΔLBD, Hs-ACVR1ΔLBD*), at

two difference concentrations, and observed no phenotypic changes as compared to full length WT mRNA injected embryos (Fig. 6A–C). We then tested whether *Dr-acvr1l/ΔLBD* or *Hs-ACVR1ΔLBD* mRNA could rescue homozygous the *acvr1l*$^{\Delta 13bp/\Delta 13bp}$ mutant C2-dorsalization phenotype. Neither *Dr-acvr1l/ΔLBD* nor *Hs-ACVR1ΔLBD* mRNA could rescue *acvr1l*$^{\Delta 13bp/\Delta 13bp}$ C2-dorsalization phenotype (Fig. 6D–H). Injection of either *Dr-acvr1l/ΔLBD* or *Hs-ACVR1ΔLBD* mRNA resulted in ~75% WT looking embryos, and ~25% C2-dorsalized embryos, as expected from a heterozygous *acvr1l*$^{\Delta 13bp/+}$ incross (Fig. 6H). We further injected *Dr-acvr1l/ΔLBD* mRNA at a 1.5-fold concentration, and again saw no rescue (Fig. 6H). To confirm that none of the phenotypically normal mRNA-injected embryos were a rescued *acvr1l*$^{\Delta 13bp/\Delta 13bp}$ embryo, we genotyped 15 individual *Dr-acvr1l/ΔLBD* mRNA-injected embryos, and 14 individual *Hs-ACVR1ΔLBD* mRNA-injected embryos and found only WT or heterozygous *acvr1l*$^{\Delta 13bp/+}$ zebrafish in ratios of roughly, 1/3 and 2/3 respectively, as expected from a heterozygous *acvr1l*$^{\Delta 13bp/+}$ incross when C2-dorsalized siblings are removed (Fig. 6I–J). The absence of even mildly less-dorsalized embryos suggests that these LBD-deletion constructs retained no functional activity and are unable to even partially rescue the homozygous *acvr1l*$^{\Delta 13bp/\ \Delta 13bp}$ C2-dorszalization phenotype. In contrast, full length WT *Dr-acvr1l* and *Hs-ACVR1* mRNA both rescued *acvr1l*$^{\Delta 13bp/\Delta 13bp}$ C2-dorsalization (Fig. 3L).

Next, we injected zebrafish and human FOP variant LBD-deletion mRNAs (*Dr-acvr1l/ΔLBD*^{R203H}, Hs-*ACVR1ΔLBD*^{R206H}) into single cell stage WT zebrafish embryos and monitored their phenotypes at 24hpf (Fig. 6K–M). Injection of *Dr-acvr1l/ΔLBD*^{R203H} mRNA at two different concentrations resulted in all WT phenotypes (Fig. 6K, Fig. 5D, Columns 4–5). In contrast, *Hs-ACVR1ΔLBD*^{R206H} mRNA injection resulted in a spectrum of ventralization phenotypes (V1-V5) (**Fig. 6L-M**, Fig. 5D, Columns 6–7). These results showed that Hs-ACVR1^{R206H} lacking a LBD still retained its ability to induce zebrafish embryonic ventralization. Although assayed in separate experiments, as compared to full length *Hs-ACVR1*^{R206H} mRNA, injection of an equal amount of *Hs-ACVR1ΔLBD*^{R206H} mRNA yielded a significantly higher proportion of less severe ventralization phenotypes (V1-V2 plus WT, and lower proportion of severe ventralization phenotypes (V3-V5) ($p=0.0297$) (Fig. 5D, Columns 6–7, Fig. 2Q, Column 4). Consistent with previously published *in vitro* and *in vivo* data, this data suggests that LBD deleted Hs-ACVR1^{R206H} exhibits reduced signaling compared to full length *Hs-ACVR1*^{R206H} [9,20,52]. These data also show that the LBD deleted Dr-Acvr1l^{R203H} does not show ventralization activity.

Acvr2 is a required type 2 signaling partner for human ACVR1^{R206H} in early embryonic zebrafish.

Next, we sought to identify Type II TGFβ family member receptor signaling partners for Hs-ACVR1^{R206H} in early embryonic zebrafish. Using our HS inducible *Tg(Hs-R206Ha)* transgenic zebrafish, we reasoned that the loss of a required Type II receptor signaling partner would inhibit or decrease ventralization of 4hpf HS embryos. Using this strategy, we demonstrated, for the first time, that Acvr2b paralogs are the main type II receptor signaling partners for Hs-ACVR1^{R206H}. Taking advantage of previously published anti-sense morpholino oligomer (MO) sequences, we performed single cell injections of MOs for the type II receptors *bmpr2a and bmpr2b, acvr2aa and acvr2ab, and acvr2ba* and *acvr2bb*

[55,56], into *Tg(Hs-R206Ha)* embryos followed by HS at 4hpf and phenotyping at 24hpf (Fig. 7, 8). Single clutches obtained from incrossed F2 *Tg(Hs-R206Ha)* adult zebrafish were divided into three treatments: no MO injection plus 4hpf heat-shock (No inject + HS); MO injection with no heat-shock (Inject + No HS); and MO injection plus 4hpf heat-shock (Inject + HS). We also included statistical analyses of HS non-transgenic siblings, and injected non-HS controls in Figure 7 (Fig. 7A). Shifts in ventralization were compared directly between injected and non-injected heat-shocked siblings from the same clutch (Fig. 7A). Furthermore, F2 breeding pairs were kept constant (Crosses 1–3), providing additional means of comparison between different injection sets (Fig. 7A). Injection of control MO yielded no shift in HS induced ventralization severity and had no effect on non-HS embryos (Fig. 7A, Fig. 8A). *HS-Tg(Hs-R206Ha)* progeny typically yielded V4.5 and V5 ventralized phenotypes (Fig. 7B–C), using the V4.5 designation to indicate ventralized phenotypes that appeared intermediate in severity to V4 and V5 (Fig. 7B–D). V4.5-ventralized embryos displayed a complete lack of anterior structures, a divided yolk, and a spindle-like posterior half.

Surprisingly, co-injection of *bmpr2a* and *bmpr2b* MOs increased, rather than decreased, the ventralization severity of *HS-Tg(Hs-R206Ha)*-mCherry positive embryos (Fig. 7A, D-E, Fig. 8A). In contrast to the V4.5 and V5 ventralized embryos observed in the non-injected HS group, 48% of co-injected embryos displayed a more severe V5+ ventralization phenotype (Fig. 7E–G), which was determined to be statistically significant (Figure 7A, set 2).” V5+ ventralized embryos displayed a clear spindle form, reminiscent of V5-ventralization, however were consistently reduced in size and showed partial degradation by 24hpf, suggesting arrested development. Non-HS *bmpr2a/bmpr2b* MO co-injected embryos exhibited a spectrum of dorsalization phenotypes (Fig. 8A) that did not resemble traditional C1-C5 dorsalization phenotypes and were therefore designated as B1-B5 (Fig. 8B–C). As previously described, mild dorsalization (C1-C2) consists of ventral tail fin and vein defects, whereas moderate dorsalization consists of a loss of ventral structures and twisting of the trunk. C5-dorsalized embryos lack all anterior and posterior tissues [37,39]. In contrast, *bmpr2a/bmpr2b* knockdown phenotypes retained ventral structures (tail fin, vein) until the moderate to severe categories (B3-B5), which exhibited significantly reduced anterior (head) and posterior (tail) structures. Severe trunk twisting was observed in moderate and severe categories (B3-B5), and mild categories showed ventral axis bending (B1-B2). In addition, a smaller percentage of *HS-Tg(Hs-R206Ha)* embryos with increased ventralization (V5+) phenotypes were observed when either *bmpr2a*, or *bmpr2b* MOs were each injected alone, as compared to injected together (Fig. 8).

In contrast to the observed *bmpr2* MO phenotypes, when all four *acvr2* MOs (*acvr2aa, acvr2ab, acvr2ba, acvr2bb*) were co-injected, we observed a dramatic decrease in the number and severity of 24hpf ventralized *HS-Tg(Hs-R206Ha) mCherry*-positive embryos (Fig. 7A). These results were confirmed by independent injections into two different *Tg(Hs-R206Ha)* incrossed clutches (Cross 2 and Cross 3), with no significant differences ($p>0.9999$) (Fig. 7A). In contrast to the V4.5- and V5-ventralized embryos observed in non-injected *HS-Tg(Hs-R206Ha)* controls, we observed only a small percentage of less severe V3 and V4 ventralized embryos, while the rest exhibited dorsalization phenotypes (C2-C5) (Fig. 7F–G, Fig. 8D). Therefore, the majority of *acvr2* MO-injected HS-*Tg(Hs-*

R206Ha)-mCherry expressing embryos (**Cross 2: 64.34%, Cross 3: 74%)** did not show any ventralization phenotype at all (Fig 7A). As expected, non-HS, *acvr2* MO co-injected (and HS, mCherry-negative) embryos also showed a spectrum of dorsalization phenotypes (Fig. 8A). To address concerns of embryo toxicity when injecting four *acvr2a* MOs (totaling 10ng/embryo), we injected the control MO at 2x concentration into wt embryos (totaling 16.33ng/embryo) and observed normal embryonic development (Fig. 8A).

Injection of *acvr2aa* or *acvr2ab* MO individually, or co-injection of *acvr2aa* and *acvr2ab* MOs together (at 1x or 2x concentration), yielded no shift in the ventralization phenotypes of HS-*Tg(Hs-R206Ha)*, and no phenotype at all in non-HS *Tg(Hs-R206Ha)*-mCherry embryos (Fig. 7A, Fig. 8A). In contrast, co-injection of *acvr2ba* and *acvr2bb* MOs together (at 1x or 0.5x concentration) yielded a significant shift towards less severe ventralization phenotypes in *HS-Tg(Hs-R206Ha)-mCherry* embryos (Fig. 7A). In contrast to the V4.5 and V5 ventralized embryos present in non-injected HS controls, we observed a large portion of less severe ventralization phenotypes (V1-V4) and a small portion of dorsalization phenotypes in *HS-Tg(Hs-R206Ha)*-mCherry embryos (C2-C4) (Fig. 7A). Injection of *acvr2ba* or *acvr2bb* MO individually yielded only a minor shift to less ventralized phenotypes in *HS-Tg(Hs-R206Ha)-mCherry* embryos, from V4.5/V5 to mainly V4 and V3, with no *mCherry*-positive embryos displaying dorsalization phenotypes (Fig. 8A). Non-HS *acvr2ba/acvr2bb* MO co-injected embryos showed mild dorsalization phenotypes (C1-C3), indicating their requirement for early embryonic zebrafish development, which however may function independently of WT Acvr1l (Fig. 8A).

Together, these results indicated that Hs-ACVR1^{R206H} complexes with one or more Acvr2 paralogs to induce ventralization of early embryonic zebrafish, and that Acvr2ba and Acvr2bb may be able to compensate for Acvr2aa and Acvr2ab, but not the reverse (Fig. 9). To assess if differences in knockdown efficiency or receptor expression may be responsible for the observed differences in *acvr2aa/ab* knockdown versus *acvr2ba/bb* knockdown, we tested the injection of *acvr2aa/ab* MOs at 2x concentration, and *acvr2ba/bb* MOs at 0.5x concentration and observed no statistically significant differences (P>0.9999) (Fig. 7A, Fig. 8A). In contrast, Bmpr2a and Bmpr2b appear to compete with Hs-ACVR1^{R206H} signaling, with more ventralized V5+ phenotypes observed when *bmpr2a/bmpr2b* MO injected embryos, perhaps via sequestering Hs-ACVR1^{R206H} in a non-functional complex and/or via competition for ligand and/or downstream signaling molecules (Fig. 9).

Discussion

Functional differences between human ACVR1^{R206H} and zebrafish Acvr1l^{R203H}

Our experimental results show that Hs-ACVR1^{R206H} exhibits upregulated BMP signaling in early embryonic zebrafish, while the orthologous zebrafish Dr-Acvr1l^{R203H} variant does not. Injection of *Hs-ACVR1^{R206H}* mRNA and expression of HS-*Tg(Hs-R206Ha)* both cause ventralization of early embryonic zebrafish. In contrast, injection of *Dr-acvr1l^{R203H}* mRNA, HS-*Tg(Dr-R203Ha)*, and maternal/zygotic *acvr1l$^{R203H/R203H}$* mutant embryos show no altered phenotypes. Furthermore, *HS-Tg(Dr-R203Ha)* expression can rescue homozygous *acvr1l$^{\Delta 13bp/\Delta 13bp}$* mutants indicating the WT function of the Dr-Acvr1l^{R203H} variant. Further elucidation of mechanisms contributing to the functional differences of Dr-Acvr1l^{R203H}

and Hs-ACVR1^{R206H} variants may provide useful insight into how to regulate deleterious Hs-ACVR1^{R206H} signaling in FOP patients.

Our chimeric Hs-ACVR1^{R206H}/Dr-Acvr1l^{R203H} expression studies showed that the functional differences of Hs-ACVR1^{R206H} and Dr-Acvr1l^{R203H} is mediated by the GS and/or KD domains. These results may reflect (1) altered binding affinity of the FKBP12/FKBP1A inhibitor proteins to the unphosphorylated GS-rich domain, and/or (2) altered activity of the KD to phosphorylate downstream Smad1/5/8 signaling partners [10–12,15–18]. The amino acid sequence identity of the GS domains of Dr-Acvr1l and Hs-ACVR1 is 97% (29/30 amino acids), with a single conserved amino acid substitution (Leucine and Methionine, both aliphatic non-polar) [61]. Therefore, while we do not predict differential binding affinity for FKBP12/FKBP1A, this would need to be tested empirically. The amino acid sequence identity of the KD of Dr-Acvr1l and Hs-ACVR1 is 84%.

We do not predict that the observed functional differences are due to the zebrafish ortholog's inability to phosphorylate downstream Smad1/5. Our previously published results using a Dr-Acvr1l^{Q204D} variant, an amino acid substitution immediately next to the Dr-Acvr1l^{R203H} variant, is constitutively active as predicted, and when expressed in embryonic zebrafish results in a ventralized phenotype and upregulated pSmad1/5 signaling .

The complete lack of ventralization by Dr-Acvr1l^{R203H} may also reflect differences in activation by BMP or Activin ligands. Evidence against this includes the fact that the Hs-ACVR1l^{R206H} ECD-TMD does not induce early embryonic ventralization when fused to the Dr-Acvr1l^{R203H} GS-KD. Furthermore, we showed that only WT Hs-ACVR1/Dr-Acvr1l, and not the Hs-ACVR1^{R206H}/Dr-Acvr1l^{R203H} variants, require the LBD. It is possible that Dr-Acvr1l^{R203H} exhibits reduced binding to and activation by the type II receptor dimer heteromeric complex. Although *in vitro* studies showed that BMP ligands have a higher affinity for type I as compared to type II receptors, Activin A and other high affinity ligands can directly bind to type II receptors [26,62,63]. As such, it would be informative to investigate 3D protein structures of the heteromeric ligand/type I receptor/type II receptor complexes of WT and FOP variants Hs-ACVR1/Dr-Acvr1l to determine whether conformational differences may account for the observed functional differences.

Ligand-independent activity of Hs-ACVR1^{R206H}

The functional consequences of removing the LBD of Hs-ACVR1^{R206H} have previously been tested *in vitro*, as measured through relative *BRE:luciferase* activity, and *in vivo* [9,20,52]. In NIH/3T3 and iMEF cells, LBD removal resulted in a statistically significant decrease in Hs-ACVR1^{R206H} activity [9,20]. Similarly, our *in vivo* studies showed that Hs-ACVR1^{R206H} lacking the LBD retained the ability to ventralize early embryonic zebrafish, but to a much lesser extent as compared to full length Hs-ACVR1^{R206H}. The fact that Hs-ACVR1^{R206H} can still function without its LBD may reflect its ability to maintain some binding to its type II receptor/ligand complex, although to a much lesser extent. It is known that under normal conditions, Activin A and other high affinity ligands directly bind to and block the LBD of type II receptors . In contrast, Hs-ACVR1^{R206H} was found to exhibit neofunction, where it is activated, not inhibited, by Activins A, AB, AC, and B [9,23,29]. We therefore propose that Activins still bind to the type II receptor signaling partner (ACVR2A, ACVR2B) in

zebrafish embryos, and that removal of the Hs-ACVR1^{R206H} LBD reduces, but does not eliminate, complex formation.

In contrast, removing the LBD from WT Dr-Acrvr1l or Hs-ACVR1 results in a loss of function. We showed that full length WT *Dr-acvr1l/Hs-ACVR1* mRNA can rescue C2-dorsalization in *acvr1l*$^{\Delta 13bp/\Delta 13bp}$ mutants, however removal of their respective LBDs prevented rescue. In agreement with these results, removing the LBD from WT Hs-ACVR1 also showed loss of activity in iMEF cells treated with BMP4, Activin A, or left untreated, as measured through relative *BRE:luciferase* activity [9]. These results emphasize that possible cell type-specific differences in Hs-ACVR1 signaling, potentially due to type II receptor, ligand or accessory protein availability, can produce variable results [9,17,20,26]. Since under normal conditions, BMP ligands exhibit higher affinity for type I versus type II receptors *in vitro* [26,62,63], it is likely that removing the LBDs of WT Hs-ACVR1 and Dr-Acvr1l prevents binding of canonical BMPs, resulting in a failure to oligomerize with type II receptor partners, thereby inhibiting signaling.

Type II receptor signaling partners for Hs-ACVR1^{R206H}

WT Hs-ACVR1 is known to oligomerize with ACVR2A, ACVR2B, and BMPR2 [26–28,64,65] (Fig. 9A). In many cell types, under normal physiological conditions, Activins will bind to type II receptor partners and act as antagonists for BMP signaling by creating dead-end complexes that sequester Hs-ACVR1 and type II receptor partners, preventing their contribution to BMP-induced signaling cascades [14,26–28,65(p2)]. In contrast, Activins act as agonists for Hs-ACVR1^{R206H}, promoting BMP-like signaling through pSmads1/5/8 . While *in vitro* assays have shown a clear requirement of type II receptors during Hs-ACVR1^{R206H} signaling, the major type II receptor signaling partner for Hs-ACVR1^{R206H} has not been confirmed[64,66]. Here, using anti-sense MOs in combination with our *HS-Tg(Hs-R206Ha)* zebrafish, we showed that Acvr2b paralogs are likely the main type II receptor signaling partners for Hs-ACVR1^{R206H} in early embryonic zebrafish (Fig. 7A, 9A–B). Although our results are consistent with Acvr2b as being required for Acvr1^{R206H} signaling in embryonic zebrafish, it is possible that there is more than one mechanism through which Acvr2b affects embryonic pattering, including acting independently of Acvr1^{R206H}.

In contrast, MO targeted depletion of both zebrafish Acvr2aa and Acvr2ab showed no effect on the ventralization phenotype of *HS-Tg(Hs-R206Ha)* embryos, (or on dorsoventral patterning in non-HS embryos), suggesting that Acvr2b paralogs can compensate for loss of Acvr2aa/ab in Hs-R206H signaling in embryonic zebrafish (Fig. 7A, 9A–B). In contrast, Acvr2aa and Acvr2ab are unable to compensate for lack of Acvr2ba/Acvr2bb, confirming the requirement for Acvr2ba/bb in Hs-ACVR1^{R206H} signaling in early embryonic zebrafish (Fig. 7A, 9A–B). Titrating MO concentrations (*acvr2aa/acvr2ab* 2x concentration, and *acvr2ba/acvr2bb* 0.5x concentration) yielded similar results, providing additional support that this observation is not simply due to differential knockdown efficiencies or receptor expression levels. We believe that Hs-ACVR1^{R206H} can also signal through Acvr2aa/Acvr2ab, although weakly, based on our results showing that knockdown of all four zebrafish Acvr2 receptors - Acvr2aa, Acvr2ab, Acvr2ba, Acvr2bb - produced the strongest decrease in Hs-ACVR1^{R206H} signaling, as measured by the less severe early embryonic

ventralization phenotypes (Fig. 7A, 9A–B). In the absence of these type II receptor partners, Activin-A induced Hs-ACVR1^{R206H} clustering and auto-activation does not occur [14]. As such, the contributions of human ACVR2A and ACVR2B to Hs-ACVR1^{R206H} signaling should be considered when designing therapeutic strategies for FOP patients.

We previously showed that zebrafish Acvr1l/Alk8 does not form *in vitro* complexes with ACVR2A/ACVR2B in the presence of Bmp2, in COS-1 cells, while BMPR1A (Alk3) does [67]. Similarly, the mammalian ortholog ACVR1/ALK2 does complex with ACVR2A/ACVR2B in myeloma cell lines in the presence of Bmp6 and −9, but not Bmp2 or −4 [27,65]. Although Acvr2aa/ab/ba/bb receptors likely interact with multiple type I receptors in the early zebrafish embryo, in this study we did not directly test their requirements for WT Acvr1l signaling [27,65,67–70]. However, Acvr2aa/ab/ba/bb knockdown does interfere Hs-ACVR1^{R206H} signaling resulting in severe C3-C5 dorsalization phenotypes in *acvr2* MO-injected HS-*Tg(Hs-R206Ha)* embryos. It is also possible that other mechanisms also contribute to the observed *acvr2aa/ab/ba/bb* MO dorsalization phenotype.

Knockdown of zebrafish Bmpr2aa and Bmpr2ab in *HS-Tg(Hs-R206Ha)* zebrafish embryos produced the opposite effect of removing Acvr2a/b, in that embryos exhibited an even stronger ventralization phenotype indicative of increased Hs-ACVR1^{R206H} signaling (Fig. 7A, 9A–B). These results suggest that the presence of Bmpr2aa/Bmpr2ab may interfere with Hs-ACVR1^{R206H} signaling, potentially by competing for ligand, accessory and/or downstream signaling partner proteins. Another possibility is that Hs-ACVR1^{R206H} does partner with Bmpr2aa/Bmpr2ab (BMPR2A), but does not initiate signaling, or produces a much weaker signaling complex, as compared to ACVR2A/ACVR2B. As such, removing Bmpr2aa and Bmpr2ab in the early zebrafish embryo could free up more Hs-ACVR1^{R206H} to partner with Acvr2b paralogs, thereby increasing signaling and ventralization. Consistent with these results, previous *in vitro* studies in myeloma cell lines showed that BMPR2 knockdown strongly potentiated Activin-induced signaling through Hs-ACVR1[65]. Myeloma cells uniquely exhibit Activin-induced signaling via WT Hs-ACVR1, as does Hs-ACVR1^{R206H} in FOP patients [65]. These results suggest that *BMPR2* overexpression strategies may be useful in dampening Hs-ACVR1^{R206H} signaling in FOP patients.

Conclusions

Here we have used early embryonic zebrafish dorsoventral patterning to interrogate functional domains and type II receptor signaling partners of the FOP-associated Hs-ACVR1^{R206H} and Dr-Acvr1l^{R203H} variants. We showed that Hs-ACVR1^{R206H} exhibits upregulated BMP signaling in early embryonic zebrafish while Dr-Acvr1l^{R203H} does not, and that this functional difference is mediated by their respective GS and Kinase domains. Elucidating the mechanisms contributing to these functional differences will likely be useful in devising strategies to decrease Hs-ACVR1^{R206H} signaling in FOP patients. We also showed that Hs-ACVR1^{R206H} retains early embryonic ventralization activity without its LBD, while WT Dr-Acvr1l and WT Hs-ACVR1 require their LBDs for proper function. Finally, we show for the first time that Acvr2b paralogs are the main type II signaling partners for Hs-ACVR1^{R206H} in the early zebrafish embryo, while Bmpr2 paralogs interfere

with Hs-ACVR1^{R206H} signaling. As such, manipulating the levels of type II receptor availability may be a potential therapeutic strategy to decrease Hs-ACVR1^{R206H} signaling in FOP patients.

Our long-term goal is to create adult zebrafish transgenic lines and endogenous CRISPR/cas9 mutants to model human FOP phenotypes. The studies described here validate new transgenic zebrafish FOP lines in the early embryo and provide new insight into signaling partners for Hs-ACVR1^{R206H} and Dr-Acvr1l^{R203H}. Now that our FOP zebrafish lines have been validated in early embryonic zebrafish, future studies will characterize signaling pathways and FOP progression in adult *Tg(Hs-R206Ha)* and *Tg(Dr-R203Ha)* transgenic lines, and in adult MZ*acvr1l*$^{R203H/R203H}$ zebrafish, using methodologies previously used by us to characterize zebrafish Dr-Acvr1l^{Q204D} variants [49,57,58]. Although early embryonic *HS-Tg(Dr-R203Ha)* and MZ*acvr1l*$^{R203H/R203H}$ zebrafish do not exhibit ventralization phenotypes, it is possible that they may exhibit heterotopic ossification and other FOP phenotypes as adults. Just as *in vitro* data can exhibit cell line-specific differences due to varied protein and receptor availability [9,17,20,26], similarly early embryonic development and adult FOP phenotypes are quite distinct. We therefore look forward to further characterization of these useful, validated *in vivo* zebrafish tools to provide new insight into mechanisms regulating human FOP.

Experimental Procedures

Zebrafish husbandry

All zebrafish used in these experiments were housed in an ALAAC approved zebrafish facility maintained at 28°C with a 14 hour light and 10 hour dark cycle, and were fed regularly [71]. All animal care and experiments were performed according to Tufts University approved IACUC protocols.

Heat-shock

Embryos were heat-shocked at 4hpf for one hour using a thermocycler, five embryos per PCR tube in 100μl of E3 media (no methylene blue).

Cloning

Heat-shock inducible constructs—To create the pDest *Tg(Hsp70:Dr-acvr1l*^{R203H}*-mCherry)* construct, site-directed mutagenesis was performed on the previously published pDest *Tg(Hsp70:Dr-acvr1l(WT)-mCherry)* construct using the Q5-SDM kit [49]. The following primers were used to create the R203H variant:

FW 5’- ACGGTTGCGCacCAGATCAGCC – 3’

REV 5’- TCTCTGAACCAGGAAGGG – 3’

The pDest *Tg(Hsp70:Hs-ACVR1*^{R206H}*-mCherry)* construct was generated using the same strategy as previously described for pDest *Tg(Hsp70:Dr-acvr1l(WT)-mCherry)* in Labonty et al. 2017[49]. Briefly, the pDest *Tg(Hsp70:Hs-ACVR1*^{R206H}*-mCherry)* construct was generated using the Tol2kit, a gateway-based cloning kit for generating Tol2 transgenesis

plasmids[72]. Three-part Gateway cloning recombination reactions were used to combine the p5E-*hsp70l* (1.5 kb hsp70l promoter, plasmid #222), the Hs-ACVR1^{R206H}, and p3E-mCherrypA (mCherry for C-terminal fusions, plus SV40 late polyA, plasmid #388). The human *ACVR1* ^{R206H} cDNA (no stop codon) was first cloned into the pDONR 221 vector (Thermofisher, #12536017). The following primers were used to amplify *Hs-ACVR1* cDNA from the pCDNA3.2 plasmid:

ACVR1 FW 5'- atggtagatggagtgatgattcttcctg-3'; and

ACVR1 REV 5'- acagtcagttttcaatttgtcgaggga-3'.

The assembled pieces were inserted into the pDestTol2pA2 (an attR4-R3 gate flanked by Tol2 inverted repeats, plasmid #394)[72].

The gateway assembly plasmid maps for *pDest Tg(hsp70l:acvr1l$^{wt/R203H}$-mCherry)* and *pDest Tg(hsp70l:ACVR1^{R206H}-mCherry)* are shown below:

Chimeric ECD-TM+GS-KD constructs.—Human ACVR1 fragments were amplified using the following primers:

FW Hs-ACVR1 ECD-TM 5'-GAA TTC ATG GTA GAT GGA GTG ATG ATT C-3'

REV Hs-ACVR1 ECD-TM 5'-A

TC GAT AGT GCC ATA CTC CAC GTC TC-3'

FW Hs-ACVR1 GS/KD 5'ATC GAT GGG CTC ATC ACC ACC AAT GTT G-3'

REV Hs-ACVR1 GS/KD 5'GCG GCC GCC TAA CAG TCA GTT TTC AAT TTG-3'

The PCR amplified fragments were then cloned into pCDNA 3.2 *Dr-acvr1l^{R203H}* using EcoR1/ClaI (Hs-ACVR1 ECD-TM), and ClaI/NotI (Hs-ACVR1 GS/KD). The constructs were fused at amino acid position 167 and 164 of the human and zebrafish protein sequences, respectively (Fig. 1K, red D and box).

Ligand-binding domain (LBD) deletion constructs—Ligand binding domains were removed using the Q5 site-directed mutagenesis kit using the following primers:

FW Dr-*acvr1l* (R203H/WT) 5'-TGC AAC GCC AAC GTC TCC AAA GAG ACC C-3'

REV Dr-*acvr1l* (R203H/WT) 5'-GTC AAT GGA GAC ATC TTT AGC TGA TGT CTG-3'

FW Hs-A*CVR1* (R206H/WT) 5'-TGT AAC AGG AAC ATC ACG GCC CAG CTG C-3'

REV *Hs-ACVR1* (R206H/WT) 3'-CAT GTA GAG TTT GGG GTT GAC CTT GGG C-3'

Amino acids 35–98, and 29–89 were removed from the Hs-ACVR1 andDr-Acvr1l proteins, respectively (Fig. 1K).

***pCDNA 3.2 acvr1l*^{R203H} expression construct.—** *Dr-acvr1l*^{R203H} cDNA was amplified from the pDest *Tg(Hsp70:Dr-acvr1l*^{R203H}*-mCherry)* and cloned into the pCR Blunt-ii-TOPO vector. A stop codon was added, and EcoRI, and NotI restriction sites, using the following primers:

FW 5'GAA TTC ATG GGG CAT TGC AGC ACC CAA-3'

REV 5'GCG GCC GCT TAG CAG TCG GTT TTG CC-3'

The *Dr-acvr1l*^{R203H} cDNA fragment was then subcloned into the pCDNA 3.2 vector using the EcoR1, and NotI restriction sites.

Other plasmids—pCS2+ WT *Dr-acvr1l* was provided by the Mullins lab [38].

pCDNA 3.2 Hs-*ACVR1(R206H & WT)* was provided by the Hsiao lab [73]. The human cDNA was obtained from FOP patient-derived human induced pluripotent stem cells (hiPSCs), kind gift of Dr. Edward Hsiao, UCSF (Barruet et al. 2016).

Plasmid Microinjections and transgenic line generation

Constructs (final concentration 25ng/μL) were co-injected with transposase RNA (final concentration of 80ng/μL) mixed with 0.2M KCl and 0.5% phenol red in one cell-stage zebrafish embryos (1–2nL volume per injection). Initial phenotypic analysis of mCherry tagged *Tg(Dr-WTa/b), Tg(Hs-R206Ha/b/c),* and *Tg(Dr-R203Ha/j/k)* was performed on F1s. MO experiments were performed on F3 clutches from incrossed F2 zebrafish. F2 fish were obtained by incrossing F1 zebrafish. To screen for transgenic lines, embryos were heat-shocked at 24hpf, and observed under fluorescence (mCherry) at 48hpf. Adult zebrafish were heat-shocked for 1 hour in a 37°C water bath and screened for fluorescence later the same day.

CTCF (Calculated Total Cell Fluorescence) calculations

CTCF images were taken at 24hpf, following heat-shock at 4hpf. For each embryo, mCherry fluorescence intensity was quantified using ImageJ, subtracting the fluorescent intensity of the background from the measured intensity of the whole image. The CTCF was calculated using Microsoft Excel with the following formula: Integrated density whole–(area whole embryo * mean fluorescence background)[74,75].

mRNA injection

All pCDNA 3.2 vector expression constructs (*Hs-ACVR1(R206H, WT, R206HΔLBD, WTΔLBD*), *Dr-acvr1l*(*R203H*, *R203HΔLBD*), *Hs-Dr-ECD-TM+Hs-GS/KD, Hs-ECD-TM+Dr-GS/KD)* were linearized with DraIII, and *in vitro* transcribed using the T7 mMessage Machine kit. pCS2+ *Dr-acvr1l* and pCS2+ *Dr-acvr1lΔLBD* were linearized with NotI and *in vitro* transcribed using the Sp6 mMessage Machine kit. Following *in vitro* transcription, mRNAs were extracted using phenol/chloroform, and precipitated using isopropanol. Individual final mRNA injection concentrations are described in the results section. mRNA was mixed with 0.2M KCl and 0.5% phenol red and injected into one cell-stage zebrafish embryos.

CRISPR/Cas9 Homology Directed Repair strategy

The *acvr1l* CRISPR /Cas9 HDR R203H allele, and *acvr1l*$^{\Delta 13bp}$ allele were created by co-injecting the following:

gRNA1 (40ng/μL final), Target Sequence: 5'-TGCGCGGCAGATCAGCCTGGTGG-3'

gRNA2 (40ng/μL final), Target Sequence: 5'-TGGTTCAGAGAACGGTTGCGCGG-3'

ssODN (60ng/ul final) à 5'-GCC CTT CCT GGT TCA GAG AAC GGT TGC CCA CCA GAT CAG CCT GGT GGA GTG TGT TGG TAA GAC AAA-3'

TriLink CleanCap cas9 mRNA (300ng/ul final), 0.5% phenol red, 0.2M KCl

F1 heterozygous zebrafish (from individual F0 founder zebrafish) were sequenced to confirm the desired nucleotide changes. All subsequent *acvr1l*^{R203H} zebrafish are the result of incrossed sequenced F1 zebrafish. gRNAs were cloned into the pDR274 plasmid, linearized with HindIII, and in vitro transcribed using the T7 Megashortscript kit. The homology directed repair strategy is similar to those tested in Prykhozhij et al. 2018[76].

Genotyping

Adult and larval zebrafish were genotyped for *acvr1l*$^{\Delta 13bp}$, *acvr1l*^{R203H} alleles using the following primers:

FW 5'-CCA CGA ACT GCC AAG GAT TA-3'

REV 5'- CGA GTC TGA CGT ACT TCC AATG-3'

Following PCR, HhaI enzyme was added directly to the PCR tube and digested at 37°C for 2 hours.

CRISPR/Cas9 Homology Directed Repair screening statistics

To recover the *acvr1l* endogenous R203H allele, 26 F0 fish were screened. 30 F1 embryos were screened per F0, pooled in batches of 10 embryos for genotyping. From PCR/restriction digest samples that showed loss of the HhaI restriction site, we recovered 4 F0s transmitting INDEL alleles (15.4%), 1 F0 transmitting an imperfect R203H allele (INDEL causing frameshift) (3.8%), and 1 F0 transmitted an R203H allele with synonymous SNP (3.8%).

Anti-sense Morpholino (MO) injections.

All MOs used were previously published [55,56]. Standard control MO was used.

acvr2aa ATG MO—3 ng (5′-CCAGCTTTGTTGCAGGTCCCATTTT-3′)

acvr2ab splice MO—4 ng (5′-TGGCTGCACACAAACACAGATTAAT-3′),

acvr2ba ATG MO—2 ng (5′-TGAGCAGAGAAGCGAACATATTCCT-3′),

acvr2bb ATG MO—1 ng (5′-AGCCAGCCAGGGAACAAACATATTC-3′)

bmpr2a ATG MO3—0.5mM (5′-TGTTATTCGGCCTTCAACTGCCATG-3′)

bmpr2b ATG MO3—0.1mM (5′-CACTCTCATCCTGCTGCCGCTTCTG-3′)

Control MO— 0.5mM

Mutant strains

laf^{tm110} mutant

Gene: *acvr1l*, Mutation annotation: tm110b (Provided by Mullins lab)

RT-PCR

Total RNA was extracted using Trizol, and cDNA was made using the Superscript III First-strand synthesis kit. The following primers were used for RT-PCR:

acvr1l Exon 5 FW 5'- GAC ACT GAA CAG GGG GCC ATC GAT – 3'

acvr1l Exon 7 Rev 5'- CCA TTG ACC TCT CCA CAC TTC ACC G – 3'

β-actin FW 5'- CGA GCA GGA GAT GGG AAC C – 3'

β-actin Rev 5'- CAA CGG AAA CGC TCA TTG C – 3'

Zebrafish Protein Extracts

HS-*Tg(Dr-acvr1l-WTa)*, HS-*Tg(Hs-R206H)* and Hs-*Tg(Dr-R203H)* zebrafish were validated as follows. Embryos from individual adult pairs were heat-shocked (HS) at 4 hours post fertilization (hpf) for 1 hour at 37°C. Embryos were then screened the next day for ventralization phenotypes and mCherry expression. Individual adult pairs were then validated by repeating this process a second time. Next, embryos generated from validated adult pairs were allowed to develop to 5 days post fertilization (dpf), at which time they were HS for 1 hour at 37°C and screened for mCherry-tagged transgene expression. Validated mCherry positive embryos were collected for protein extraction 5–6 hours after heat-shock.

Pools of 30 mCherry-positive 5dpf zebrafish were flash frozen in liquid nitrogen then homogenized on ice into a fine powder and dissolved in chilled RIPA lysis Buffer (Sigma Cat. No. #20–188) containing protease and phosphatase inhibitors [cOmplete Tablets, Roche; and PhosSTOP, Roche] (150 µL per 30 pooled larvae) and mixed well. The protein lysates were incubated on ice for at least 15 minutes with rocking, and then centrifuged at 11,000 rpm at 4°C for 15 minutes. The supernatant was transferred into a new Eppendorf tube and stored at −80°C until use. Total protein concentrations were quantified using BCA Protein Assay (Thermofisher #23225) and a SpectraMax i3x as per manufacturers' protocols.

Western Blots

Protein lysates were thawed on ice, and 25 ug of each protein sample was aliquoted into clean Eppendorf tubes. Loading buffer (4X) and RIPA (as needed) was added to a 15

uL volume, and the samples were boiled for 5 mins and centrifuged at 11,000 rpm for 2 minutes at 4°C . The supernatants were loaded onto 8–16% acrylamide gradient gels (Mini-PROTEAN TGX Gels, Bio-Rad #4561105) and electrophoresed at 130V for 1 hour and 10 min. Chameleon Duo (Li-Cor #928–60000, Lincoln, NE,) served as the protein marker ladder. Protein transfer to PVDF membrane was done at 70V for 1 hour, and PVDF membranes were blocked for 1 hour at Room Temperature (RT) in 5% BSA-TBST. The membranes were probed overnight at 4°C with 1:1000 anti-pSmad1/5 (Cell Signaling Technology (CST) #9516) and 1:2000 anti-mCherry antibodies in 5% BSA in TBST on a rocker. The membranes were washed 3x in TBST (5 min/wash) and then incubated for 1 hour at room RT in the dark, with secondary antibodies Anti-rabbit IgG (H+L) at 1:1000 (CST #7074) and Anti-mouse IgG (H+L) at 1:1000 (CST #5470) in 5% BSA -TBST. The membranes were imaged using Odyssey CLx (Li-Cor,Lincoln, NE). Membranes were scanned on Auto using both the 700 and 800 channels with 169 μm resolution on medium for scan speed/quality and 0.0 mm for focus offset. Prior to the second round of primary antibody incubation, membranes were stripped (Thermo scientific #46430; 37°C for 15 minutes), washed (2x with TBST; 5 min/wash) and blocked (5% BSA at RT for 1 hour). Membranes were then incubated with mouse anti-beta tubulin antibody (Sigma #T5201, 1:10,000) in 5% BSA- TBST overnight at 4°C. Re-probed blots were washed, incubated with secondary antibody and imaged as described above.

Western Blot Analysis

Western blot membrane images were analyzed using Fiji (ImageJ). Color images were converted to greyscale (8-bit type) prior to analysis. “Set Measurements” was selected under the “Analyze” tab, and only the “Mean gray value” checkbox was selected. A region of interest (ROI) was then defined using the rectangle tool. The size of the ROI encompassed the largest band being analyzed. The rectangle was placed on the band of interest, and band intensity was measured by pressing “Ctrl M” (“Command M” for Mac users). The same rectangle was used, and the same steps were repeated to measure the intensity of the bands in the other lanes. The background signal for each band was also measured by placing the same rectangle above or below each of the measured bands. Consistency was practiced by ensuring that if the rectangle was placed above/below a band for background signal measurement, the same was done for all bands in the blot. The corrected and adjusted band intensity values were calculated as follows:

Corrected band intensity = band intensity – background

Adjusted band intensity = corrected band intensity / corrected band intensity of the loading control

Statistical Analyses

For Fig. 2, 3, 5, and 6 embryos for each group were phenotypically scored from 1 (WT/Other) – 6 (C5). For Figure 8, embryos were phenotypically scored from 1 (V5+) - 7 (C5), using 0.5 intervals. The sum of the phenotypic scores per group was determined. From this sum, the average phenotypic score per group was calculated. The average phenotypic score of each group was then compared to each other and/or the control. Unpaired non-parametric

(Mann-Whitney) two-tailed t-test was done to compare the phenotypic scores between two groups. For analyses with more than two groups, Kruskal-Wallis test with Dunn's correction for multiple tests was performed to compare the phenotypic scores between the groups. The proportion of embryos presenting each phenotype per group is included. For Western Blot analysis, 2–3 biological replicates were averaged from 3 technical replicates. One-Way ANOVA was performed with Tukey's correction for multiple tests. Adjusted p-values after multiple tests correction are reported and significance was set at $p < 0.05$. GraphPad Prism 9.0.2 was used to perform statistical tests and generate graphs.

Acknowledgments.

We would like to acknowledge Dr. Nathan Lawson for his help in designing the strategy used for *acvr1l*^{R203H} homology-directed repair. We would like to acknowledge Dr. Melissa LaBonty for cloning the *Tg(Hs-R206H)* construct and validating the gRNAs used for homology-directed repair. We would like to acknowledge Alex Cintolo for injecting FOs and identifying the *Tg(Dr-R203Ha)* transgenic line. We would like to acknowledge Dr. Venkatesh Krishna for his contributions towards cloning the *Tg(Hs-R206H)* construct and screening for *Tg(Dr-R203H)* transgenic lines. We would like to acknowledge Hannah Rudolph, Liana Monderer, Soo Min Kim, and Kyra Mills for their contributions to genotyping the *Dr-acvr1l*$^{\Delta 13bp}$ and *Dr-acvr1l*^{R203H} lines. We would like to acknowledge the Mullins lab for providing the *laf*^{tm110b} mutant and the pCS2+ *acvr1l* plasmid, and the Hsiao lab for providing the pCDNA 3.2 *Hs-ACVR1(R206H & WT)* plasmids. We would like to thank Dr. Aris Economides for his personal communications. We thank Dr. Peter Geck, M.D. for his help with Western Blots, and Dr. Alexandra Poltorak and Lab for help in imaging our Western Blots.

Grant Sponsor: NIH/NIAMS

Grant Number: R21 AR072085 (PCY)

References

1. Hüning I, Gillessen-Kaesbach G. Fibrodysplasia Ossificans Progressiva: Clinical Course, Genetic Mutations and Genotype-Phenotype Correlation. MSY. 2014;5(5):201–211. doi:10.1159/000365770
2. Kaplan FS. The skeleton in the closet. Gene. 2013;528(1):7–11. doi:10.1016/j.gene.2013.06.022 [PubMed: 23810943]
3. Shore EM, Xu M, Feldman GJ, et al. A recurrent mutation in the BMP type I receptor ACVR1 causes inherited and sporadic fibrodysplasia ossificans progressiva. Nat Genet. 2006;38(5):525–527. doi:10.1038/ng1783 [PubMed: 16642017]
4. Kaplan F, McCluskey W, Hahn G, Tabas J, Muenke M, Zasloff M. Genetic Transmission of Fibrodysplasia Ossificans Progressiva. Report of a Family. The Journal of Bone and Joint Surgery-american Volume. 1993;75(8):1214–1220. [PubMed: 8354680]
5. Kaplan FS, Zasloff MA, Kitterman JA, Shore EM, Hong CC, Rocke DM. Early Mortality and Cardiorespiratory Failure in Patients with Fibrodysplasia Ossificans Progressiva: The Journal of Bone and Joint Surgery-American Volume. 2010;92(3):686–691. doi:10.2106/JBJS.I.00705 [PubMed: 20194327]
6. Kaplan FS, Pignolo RJ, Shore EM. From mysteries to medicines: drug development for fibrodysplasia ossificans progressive. Expert Opin Orphan Drugs. 2013;1(8):637–649. doi:10.1517/21678707.2013.825208 [PubMed: 24800180]
7. Kaplan FS, Xu M, Seemann P, et al. Classic and atypical fibrodysplasia ossificans progressiva (FOP) phenotypes are caused by mutations in the bone morphogenetic protein (BMP) type I receptor ACVR1. Hum Mutat. 2009;30(3):379–390. doi:10.1002/humu.20868 [PubMed: 19085907]
8. Zhang W, Zhang K, Song L, et al. The Phenotype and Genotype of Fibrodysplasia Ossificans Progressiva in China: A Report of 72 Cases. Bone. 2013;57(2):386–391. doi:10.1016/j.bone.2013.09.002 [PubMed: 24051199]
9. Haupt J, Xu M, Shore EM. Variable signaling activity by FOP ACVR1 mutations. Bone. 2018;109:232–240. doi:10.1016/j.bone.2017.10.027 [PubMed: 29097342]

10. Huang F, Chen YG. Regulation of TGF-β receptor activity. Cell & Bioscience. 2012;2(1):9. doi:10.1186/2045-3701-2-9 [PubMed: 22420375]
11. Massagué J. Receptors for the TGF-beta family. Cell. 1992;69(7):1067–1070. doi:10.1016/0092-8674(92)90627-o [PubMed: 1319842]
12. Zinski J, Tajer B, Mullins MC. TGF-β Family Signaling in Early Vertebrate Development. Cold Spring Harb Perspect Biol. 2018;10(6). doi:10.1101/cshperspect.a033274
13. Little SC, Mullins MC. Bone morphogenetic protein heterodimers assemble heteromeric type I receptor complexes to pattern the dorsoventral axis. Nat Cell Biol. 2009;11(5):637–643. doi:10.1038/ncb1870 [PubMed: 19377468]
14. Ramachandran A, Mehić M, Wasim L, et al. Pathogenic ACVR1R206H activation by Activin A-induced receptor clustering and autophosphorylation. EMBO J. 2021;40(14):e106317. doi:10.15252/embj.2020106317
15. Machiya A, Tsukamoto S, Ohte S, et al. Effects of FKBP12 and type II BMP receptors on signal transduction by ALK2 activating mutations associated with genetic disorders. Bone. 2018;111:101–108. doi:10.1016/j.bone.2018.03.015 [PubMed: 29551750]
16. Chen YG, Liu F, Massague J. Mechanism of TGFbeta receptor inhibition by FKBP12. EMBO J. 1997;16(13):3866–3876. doi:10.1093/emboj/16.13.3866 [PubMed: 9233797]
17. Song GA, Kim HJ, Woo KM, et al. Molecular consequences of the ACVR1(R206H) mutation of fibrodysplasia ossificans progressiva. J Biol Chem. 2010;285(29):22542–22553. doi:10.1074/jbc.M109.094557 [PubMed: 20463014]
18. Wang T, Li BY, Danielson PD, et al. The Immunophilin FKBP12 Functions as a Common Inhibitor of the TGFβ Family Type I Receptors. Cell. 1996;86(3):435–444. doi:10.1016/S0092-8674(00)80116-6 [PubMed: 8756725]
19. Groppe J, Hinck CS, Samavarchi-Tehrani P, et al. Cooperative assembly of TGF-beta superfamily signaling complexes is mediated by two disparate mechanisms and distinct modes of receptor binding. Mol Cell. 2008;29(2):157–168. doi:10.1016/j.molcel.2007.11.039 [PubMed: 18243111]
20. Haupt J, Deichsel A, Stange K, et al. ACVR1 p.Q207E causes classic fibrodysplasia ossificans progressiva and is functionally distinct from the engineered constitutively active ACVR1 p.Q207D variant. Hum Mol Genet. 2014;23(20):5364–5377. doi:10.1093/hmg/ddu255 [PubMed: 24852373]
21. Gupta A, Zimmermann MT, Wang H, et al. Molecular characterization of known and novel ACVR1 variants in phenotypes of aberrant ossification. American Journal of Medical Genetics Part A. 2019;179(9):1764–1777. doi:10.1002/ajmg.a.61274 [PubMed: 31240838]
22. Mucha BE, Hashiguchi M, Zinski J, Shore EM, Mullins MC. Variant BMP receptor mutations causing fibrodysplasia ossificans progressiva (FOP) in humans show BMP ligand-independent receptor activation in zebrafish. Bone. 2018;109:225–231. doi:10.1016/j.bone.2018.01.002 [PubMed: 29307777]
23. Hatsell SJ, Idone V, Wolken DMA, et al. ACVR1R206H receptor mutation causes fibrodysplasia ossificans progressiva by imparting responsiveness to activin A. Sci Transl Med. 2015;7(303):303ra137. doi:10.1126/scitranslmed.aac4358
24. Le VQ, Wharton KA. Hyperactive BMP signaling induced by ALK2(R206H) requires type II receptor function in a Drosophila model for classic fibrodysplasia ossificans progressiva. Dev Dyn. 2012;241(1):200–214. doi:10.1002/dvdy.22779 [PubMed: 22174087]
25. Wang RN, Green J, Wang Z, et al. Bone Morphogenetic Protein (BMP) signaling in development and human diseases. Genes & Diseases. 2014;1(1):87–105. doi:10.1016/j.gendis.2014.07.005 [PubMed: 25401122]
26. Aykul S, Martinez-Hackert E. Transforming Growth Factor-β Family Ligands Can Function as Antagonists by Competing for Type II Receptor Binding. J Biol Chem. 2016;291(20):10792–10804. doi:10.1074/jbc.M115.713487 [PubMed: 26961869]
27. Olsen OE, Wader KF, Hella H, et al. Activin A inhibits BMP-signaling by binding ACVR2A and ACVR2B. Cell Commun Signal. 2015;13:27. doi:10.1186/s12964-015-0104-z [PubMed: 26047946]
28. Wiater E, Vale W. Inhibin is an antagonist of bone morphogenetic protein signaling. J Biol Chem. 2003;278(10):7934–7941. doi:10.1074/jbc.M209710200 [PubMed: 12493742]

29. Alessi Wolken DM, Idone V, Hatsell SJ, Yu PB, Economides AN. The obligatory role of Activin A in the formation of heterotopic bone in Fibrodysplasia Ossificans Progressiva. Bone. 2018;109:210–217. doi:10.1016/j.bone.2017.06.011 [PubMed: 28629737]
30. Shen Q, Little SC, Xu M, et al. The fibrodysplasia ossificans progressiva R206H ACVR1 mutation activates BMP-independent chondrogenesis and zebrafish embryo ventralization. J Clin Invest. 2009;119(11):3462–3472. doi:10.1172/JCI37412 [PubMed: 19855136]
31. Derynck R, Akhurst RJ. Differentiation plasticity regulated by TGF-beta family proteins in development and disease. Nat Cell Biol. 2007;9(9):1000–1004. doi:10.1038/ncb434 [PubMed: 17762890]
32. Graff JM. Embryonic Patterning: To BMP or Not to BMP, That Is the Question. Cell. 1997;89(2):171–174. doi:10.1016/S0092-8674(00)80196-8 [PubMed: 9108472]
33. Kishigami S, Mishina Y. BMP signaling and early embryonic patterning. Cytokine Growth Factor Rev. 2005;16(3):265–278. doi:10.1016/j.cytogfr.2005.04.002 [PubMed: 15871922]
34. Little SC, Mullins MC. Extracellular modulation of BMP activity in patterning the dorsoventral axis. Birth Defects Res C Embryo Today. 2006;78(3):224–242. doi:10.1002/bdrc.20079 [PubMed: 17061292]
35. Hammerschmidt M, Pelegri F, Mullins MC, et al. Mutations affecting morphogenesis during gastrulation and tail formation in the zebrafish, Danio rerio. Development. 1996;123:143–151. [PubMed: 9007236]
36. Hild M, Dick A, Rauch GJ, et al. The smad5 mutation somitabun blocks Bmp2b signaling during early dorsoventral patterning of the zebrafish embryo. Development. 1999;126(10):2149–2159. [PubMed: 10207140]
37. Kishimoto Y, Lee KH, Zon L, Hammerschmidt M, Schulte-Merker S. The molecular nature of zebrafish swirl: BMP2 function is essential during early dorsoventral patterning. Development. 1997;124(22):4457–4466. [PubMed: 9409664]
38. Mintzer KA, Lee MA, Runke G, Trout J, Whitman M, Mullins MC. Lost-a-fin encodes a type I BMP receptor, Alk8, acting maternally and zygotically in dorsoventral pattern formation. Development. 2001;128(6):859–869. [PubMed: 11222141]
39. Mullins MC, Hammerschmidt M, Kane DA, et al. Genes establishing dorsoventral pattern formation in the zebrafish embryo: the ventral specifying genes. Development. 1996;123:81–93. [PubMed: 9007231]
40. Muraoka O, Shimizu T, Yabe T, et al. Sizzled controls dorso-ventral polarity by repressing cleavage of the Chordin protein. Nat Cell Biol. 2006;8(4):329–338. doi:10.1038/ncb1379 [PubMed: 16518392]
41. Solnica-Krezel L, Stemple DL, Mountcastle-Shah E, et al. Mutations affecting cell fates and cellular rearrangements during gastrulation in zebrafish. Development. 1996;123:67–80. [PubMed: 9007230]
42. Wilm TP, Solnica-Krezel L. Radar breaks the fog: Insights into dorsoventral patterning in zebrafish. Proc Natl Acad Sci U S A. 2003;100(8):4363–4365. doi:10.1073/pnas.0931010100 [PubMed: 12682283]
43. Gonzalez EM, Fekany-Lee K, Carmany-Rampey A, et al. Head and trunk in zebrafish arise via coinhibition of BMP signaling by bozozok and chordino. Genes Dev. 2000;14(24):3087–3092. doi:10.1101/gad.852400 [PubMed: 11124801]
44. Schulte-Merker S, Lee KJ, McMahon AP, Hammerschmidt M. The zebrafish organizer requires chordino. Nature; London. 1997;387(6636):862–863. doi:http://dx.doi.org.ezproxy.library.tufts.edu/10.1038/43092 [PubMed: 9202118]
45. Dick A, Hild M, Bauer H, et al. Essential role of Bmp7 (snailhouse) and its prodomain in dorsoventral patterning of the zebrafish embryo. Development. 2000;127(2):343–354. [PubMed: 10603351]
46. Schmid B, Furthauer M, Connors SA, et al. Equivalent genetic roles for bmp7/snailhouse and bmp2b/swirl in dorsoventral pattern formation. Development. 2000;127(5):957–967. [PubMed: 10662635]

47. Bauer H, Lele Z, Rauch GJ, Geisler R, Hammerschmidt M. The type I serine/threonine kinase receptor Alk8/Lost-a-fin is required for Bmp2b/7 signal transduction during dorsoventral patterning of the zebrafish embryo. Development. 2001;128(6):849–858. [PubMed: 11222140]
48. Payne TL, Postlethwait JH, Yelick PC. Functional characterization and genetic mapping of alk8. Mechanisms of Development. 2001;100(2):275–289. doi:10.1016/S0925-4773(00)00541-4 [PubMed: 11165484]
49. LaBonty M, Pray N, Yelick PC. A Zebrafish Model of Human Fibrodysplasia Ossificans Progressiva. Zebrafish. 2017;14(4):293–304. doi:10.1089/zeb.2016.1398 [PubMed: 28394244]
50. Alexander C, Zuniga E, Blitz IL, et al. Combinatorial roles for BMPs and Endothelin 1 in patterning the dorsal-ventral axis of the craniofacial skeleton. Development. 2011;138(23):5135–5146. doi:10.1242/dev.067801 [PubMed: 22031543]
51. Collery RF, Link BA. Dynamic Smad-mediated BMP signaling revealed through transgenic zebrafish. Dev Dyn. 2011;240(3):712–722. doi:10.1002/dvdy.22567 [PubMed: 21337469]
52. Allen RS, Tajer B, Shore EM, Mullins MC. Fibrodysplasia ossificans progressiva mutant ACVR1 signals by multiple modalities in the developing zebrafish. Ackert-Bicknell C, Cheah KSE, Knaus P, eds. eLife. 2020;9:e53761. doi:10.7554/eLife.53761
53. Hammerschmidt M, Mullins MC. Dorsoventral Patterning in the Zebrafish: Bone Morphogenetic Proteins and Beyond. In: Solnica-Krezel L, ed. Pattern Formation in Zebrafish. Results and Problems in Cell Differentiation. Springer; 2002:72–95. doi:10.1007/978-3-540-46041-1_5
54. Wentworth KL, Lalonde RL, Groppe JC, et al. Functional Testing of Bone Morphogenetic Protein (BMP) Pathway Variants Identified on Whole-Exome Sequencing in a Patient with Delayed-Onset Fibrodysplasia Ossificans Progressiva (FOP) Using ACVR1R206H-Specific Human Cellular and Zebrafish Models. Journal of Bone and Mineral Research. 2022;37(11):2058–2076. doi:10.1002/jbmr.4711 [PubMed: 36153796]
55. Dogra D, Ahuja S, Kim HT, Rasouli SJ, Stainier DYR, Reischauer S. Opposite effects of Activin type 2 receptor ligands on cardiomyocyte proliferation during development and repair. Nat Commun. 2017;8(1):1–15. doi:10.1038/s41467-017-01950-1 [PubMed: 28232747]
56. Monteiro R, van Dinther M, Bakkers J, et al. Two novel type II receptors mediate BMP signalling and are required to establish left–right asymmetry in zebrafish. Developmental Biology. 2008;315(1):55–71. doi:10.1016/j.ydbio.2007.11.038 [PubMed: 18222420]
57. LaBonty M, Yelick PC. Animal models of fibrodysplasia ossificans progressiva. Developmental Dynamics. 2018;247(2):279–288. doi:10.1002/dvdy.24606 [PubMed: 29139166]
58. LaBonty M, Yelick PC. An Adult Zebrafish Model of Fibrodysplasia Ossificans Progressiva. Methods Mol Biol. 2019;1891:155–163. doi:10.1007/978-1-4939-8904-1_11 [PubMed: 30414131]
59. Kawabata M, Imamura T, Miyazono K. Signal transduction by bone morphogenetic proteins. Cytokine Growth Factor Rev. 1998;9(1):49–61. [PubMed: 9720756]
60. Dal-Pra S, Fürthauer M, Van-Celst J, Thisse B, Thisse C. Noggin1 and Follistatin-like2 function redundantly to Chordin to antagonize BMP activity. Developmental Biology. 2006;298(2):514–526. doi:10.1016/j.ydbio.2006.07.002 [PubMed: 16890217]
61. Bischoff R, Schlüter H. Amino acids: Chemistry, functionality and selected non-enzymatic post-translational modifications. Journal of Proteomics. 2012;75(8):2275–2296. doi:10.1016/j.jprot.2012.01.041 [PubMed: 22387128]
62. Kirsch T, Nickel J, Sebald W. BMP-2 antagonists emerge from alterations in the low-affinity binding epitope for receptor BMPR-II. EMBO J. 2000;19(13):3314–3324. doi:10.1093/emboj/19.13.3314 [PubMed: 10880444]
63. Sebald W, Nickel J, Zhang JL, Mueller TD. Molecular recognition in bone morphogenetic protein (BMP)/receptor interaction. Biol Chem. 2004;385(8):697–710. doi:10.1515/BC.2004.086 [PubMed: 15449706]
64. Bagarova J, Vonner AJ, Armstrong KA, et al. Constitutively Active ALK2 Receptor Mutants Require Type II Receptor Cooperation. Molecular and Cellular Biology. 2013;33(12):2413–2424. doi:10.1128/MCB.01595-12 [PubMed: 23572558]
65. Olsen OE, Sankar M, Elsaadi S, et al. BMPR2 inhibits activin and BMP signaling via wild-type ALK2. J Cell Sci. 2018;131(11):jcs213512. doi:10.1242/jcs.213512

66. Hino K, Ikeya M, Horigome K, et al. Neofunction of ACVR1 in fibrodysplasia ossificans progressiva. PNAS. 2015;112(50):15438–15443. doi:10.1073/pnas.1510540112 [PubMed: 26621707]

67. de Caestecker MP, Bottomley M, Bhattacharyya S, Payne TL, Roberts AB, Yelick PC. The novel type I serine-threonine kinase receptor Alk8 binds TGF-beta in the presence of TGF-betaRII. Biochem Biophys Res Commun. 2002;293(5):1556–1565. doi:10.1016/S0006-291X(02)00424-2 [PubMed: 12054694]

68. Goebel EJ, Corpina RA, Hinck CS, et al. Structural characterization of an activin class ternary receptor complex reveals a third paradigm for receptor specificity. PNAS. 2019;116(31):15505–15513. doi:10.1073/pnas.1906253116 [PubMed: 31315975]

69. Goh BC, Singhal V, Herrera AJ, et al. Activin Receptor Type IIA (ACVR2A) Functions Directly in Osteoblasts as a Negative Regulator of Bone Mass. J Biol Chem. Published online June 28, 2017:jbc.M117.782128. doi:10.1074/jbc.M117.782128

70. Lowery JW, Intini G, Gamer L, et al. Loss of BMPR2 leads to high bone mass due to increased osteoblast activity. J Cell Sci. 2015;128(7):1308–1315. doi:10.1242/jcs.156737 [PubMed: 25663702]

71. Westerfield M. The Zebrafish Book. A Guide for the Laboratory Use of Zebrafish (Danio Rerio). 5th ed. Univ. of Oregon Press, Eugene; 2007.

72. Kwan KM, Fujimoto E, Grabher C, et al. The Tol2kit: a multisite gateway-based construction kit for Tol2 transposon transgenesis constructs. Dev Dyn. 2007;236(11):3088–3099. doi:10.1002/dvdy.21343 [PubMed: 17937395]

73. Barruet E, Morales BM, Lwin W, et al. The ACVR1 R206H mutation found in fibrodysplasia ossificans progressiva increases human induced pluripotent stem cell-derived endothelial cell formation and collagen production through BMP-mediated SMAD1/5/8 signaling. Stem Cell Res Ther. 2016;7(1):115. doi:10.1186/s13287-016-0372-6 [PubMed: 27530160]

74. Felker A, Nieuwenhuize S, Dolbois A, et al. In Vivo Performance and Properties of Tamoxifen Metabolites for CreERT2 Control. PLoS One. 2016;11(4):e0152989. doi:10.1371/journal.pone.0152989

75. Burgess A, Vigneron S, Brioudes E, Labbé JC, Lorca T, Castro A. Loss of human Greatwall results in G2 arrest and multiple mitotic defects due to deregulation of the cyclin B-Cdc2/PP2A balance. Proc Natl Acad Sci U S A. 2010;107(28):12564–12569. doi:10.1073/pnas.0914191107 [PubMed: 20538976]

76. Prykhozhij SV, Fuller C, Steele SL, et al. Optimized knock-in of point mutations in zebrafish using CRISPR/Cas9. Nucleic Acids Research. 2018;46(17):e102–e102. doi:10.1093/nar/gky512 [PubMed: 29905858]

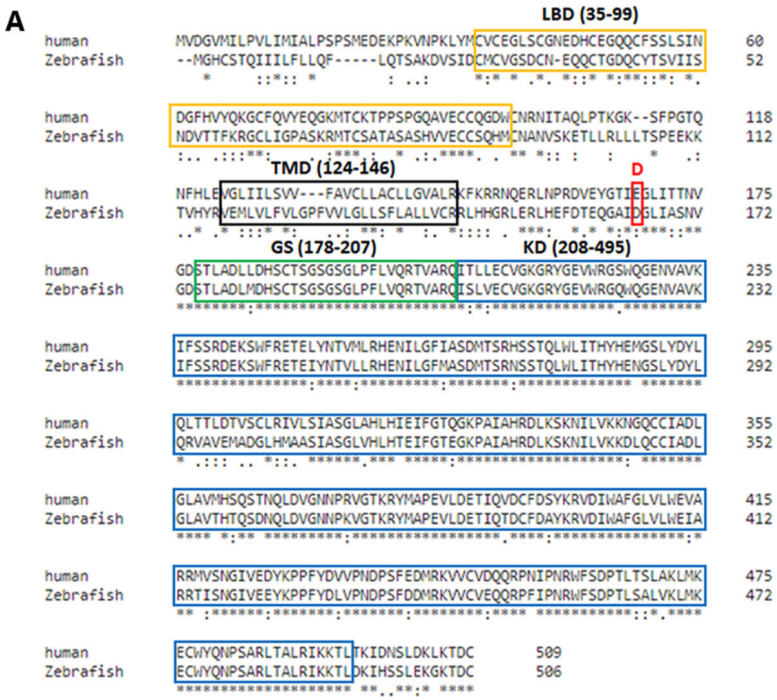

Figure 1. Human WT ACVR1 (Hs-ACVR1-WT) and zebrafish WT Acvr1l (Dr-Acvr1l-WT) amino acid sequence alignment.

The Hs-ACVR1^{R206H} and the Dr-acvr1l^{R203H} mutations are located with the GS-rich domain. LBD = Ligand Binding Domain, TMD = Transmembrane Domain, GS = GS rich domain, KD = Kinase Domain. Red box indicates fusion point for chimeric constructs (Fig. 5).

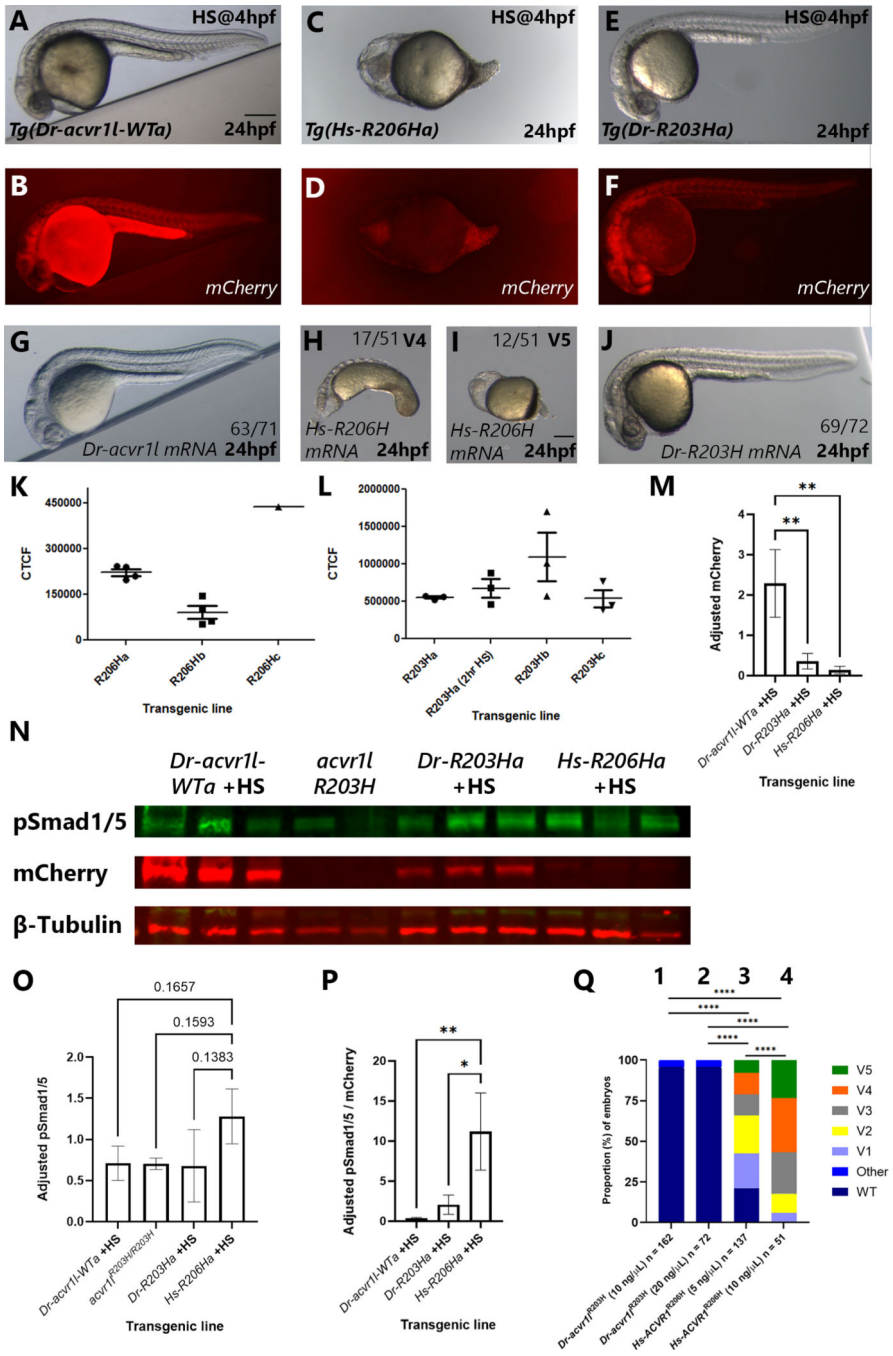

Figure 2. Zebrafish *acvr1l*^{R203H} and human *ACVR1*^{R206H} show functional differences in embryonic zebrafish.

(A-B) 24hpf *HS-Tg(Dr-acvr1l-WTa),* **(C-D)** *HS-Tg(Hs-R206Ha)*, and **(E-F)** *HS-Tg(Dr-R203Ha)* zebrafish. **(G)** *Dr-acvr1l* (WT) mRNA-injected embryos at 24hpf. **(H-I)** 24hpf *Hs-ACVR1*^{R206H} mRNA injected embryos. **(J)** 24hpf *Dr-acvr1l*^{R203H} mRNA injected embryos. N values for the highest injected mRNA concentration are shown in panels G-J. **(K-L)** CTCF analysis for *Tg(Hs-R206Ha, b, c)* and *Tg(Dr-R203Ha, b, c).* **(M)** mCherry protein levels in *HS-Tg(Dr-acvr1l-WTa)*, *HS-Tg(Dr-R203Ha),* and *HS-Tg(Hs-R206Ha)* at 5dpf

as measured through western blot analysis. **(N)** Representative western blot analysis of *HS-Tg(Dr-acvr1lWTa)*, *acvr1l*$^{R203H/R203H}$, *HS-Tg(Dr-R203Ha),* and *HS-Tg(Hs-R206Ha)* zebrafish extracts at 5dpf, following 1 hour heat-shock treatment. Blots were probed for pSmad1/5, mCherry, and β-Tubulin. **(O-P)** pSmad1/5 protein levels and pSmad1/5 levels relative to mCherry protein in *HS-Tg(Dr-acvr1l-WTa)*, *acvr1l*$^{R203H/R203H}$, *HS-Tg(Dr-R203Ha),* and *HS-Tg(Hs-R206Ha)* at 5dpf as measured through western blot analysis. Protein levels displayed in **M, O, and P** result from 2–3 biological replicates measured across 3 technical replicates. **(Q)** Ventralization phenotypes of embryos injected with full length *Dr-acvr1l*^{R203H} (Columns 1–2) or *Hs-ACVR1*^{R206H} mRNA (Columns 3–4). The proportion of embryos with each specific phenotype (color legend displayed on the right) per group is shown **(N)**. Other represents non-specific injection deformities **(N)**. Concentrations and numbers of embryos injected (n =) are presented below each bar. Each bar represents a single experiment. Significance (*) was set at $p < 0.05$. ** indicates $p < 0.01$ and **** indicates $p < 0.0001$ **(N)**. Brightfield (A, C, E, G, H, I, J), and fluorescent *mCherry* (B, D, F) images are shown. Scale bars: A-G, J = 40μm, H-I = 40μm.

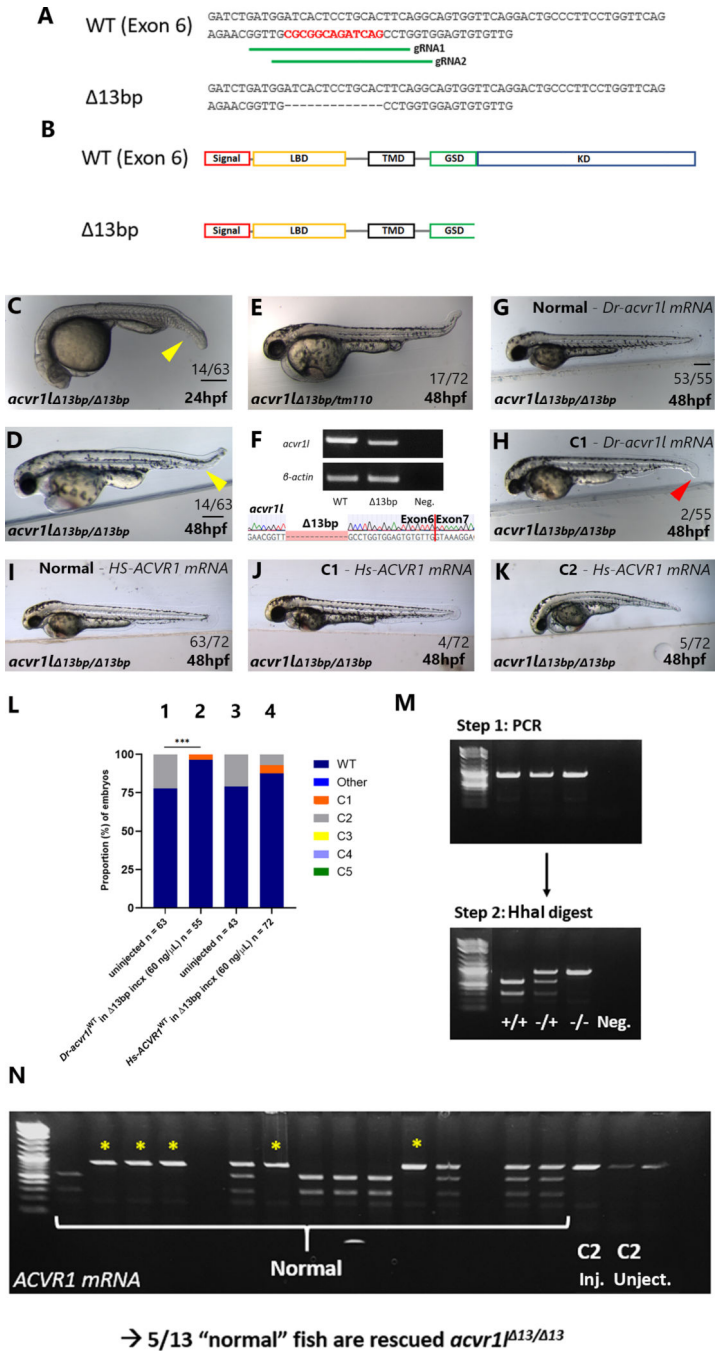

Figure 3. Zebrafish *Dr-acvr1l*$^{\Delta 13bp}$ loss-of-function allele rescue by *Dr-acvr1l* and *Hs-ACVR1* WT mRNA.

(A-B) Nucleotide sequence and protein schematic of *acvr1l* and *acvr1l*$^{\Delta 13bp}$ alleles. **(C-E)** Phenotypes of homozygous *acvr1l*$^{\Delta 13bp/\Delta 13bp}$ and trans-heterozygous *acvr1l*$^{\Delta 13bp/tm110}$ mutants at 24, 48hpf. Note the ventral tail fin defect characteristic of *acvr1l* mutant C2-dorsalized embryos (yellow arrowheads). **(F)** RTPCR of *Dr-acvr1l* from 28hpf WT and *acvr1l*$^{\Delta 13bp/\Delta 13bp}$ embryos. Amplicon spans Exon 5 – Exon 7 as confirmed by sequencing. Note mild decrease in transcript levels of *acvr1l*$^{\Delta 13bp/\Delta 13bp}$ embryos at 28hpf. **(G-H)**

WT *Dr-acvr1l* mRNA injection resulted in complete or partial rescue of homozygous *acvr1l*$^{\Delta 13bp/\Delta 13bp}$ mutants (see partially rescued median fin in C1-dorsalized embryos, red arrowhead). **(I-K)** WT *Hs-ACVR1* mRNA injected *acvr1l*$^{\Delta 13bp/\Delta 13bp}$ mutants at 48hpf. N values are shown in panels C-E, G-K. **(L)** Dorsalization phenotypes of incrossed adult heterozygous *acvr1l*$^{\Delta 13bp/+}$ progeny injected with full length WT *Dr-acvr1l* or *Hs-ACVR1* mRNA. The proportion of embryos with each specific phenotype (color legend displayed on the right) per group is shown **(L)**. Other represents non-specific injection deformities. Concentrations and numbers of embryos injected (n =) are presented below each bar **(L)**. Each bar represents a single experiment. Significance (*) was set at $p < 0.05$. ** indicates $p < 0.01$ and **** indicates $p < 0.0001$ **(L)**. **(M)** Example of 2-step genotyping (PCR amplification + HhaI restriction digest). **(N)** Genotyping of rescued homozygous *acvr1l*$^{\Delta 13bp/\Delta 13bp}$ mutants following *Hs-ACVR1* mRNA injection (yellow asterisk = *acvr1l*$^{\Delta 13bp/13bp}$). Brightfield (C, D, E, G, H, I-K) images are shown. Scale bars: C = 40μm, D-E = 40μm, G-K = 40μm.

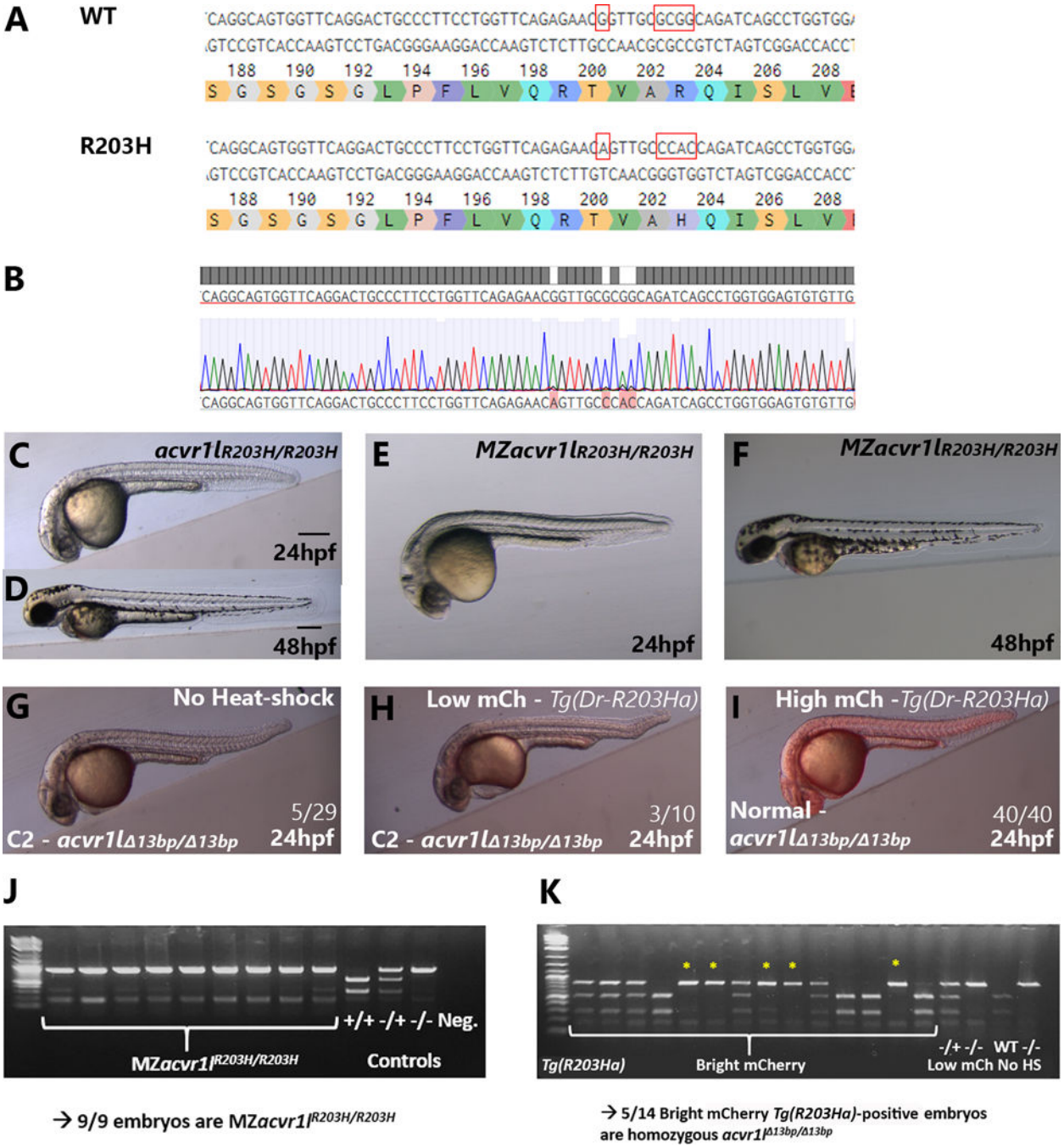

Figure 4. Zebrafish *acvr1l*^{R203H} exhibits WT *acvr1l* function in early embryonic zebrafish.

(A) Nucleotide and amino acid sequence of *acvr1l* and *acvr1l*^{R203H} alleles. Red boxes indicate altered bps in endogenous HDR created *acvr1l*^{R203H} allele (A). **(B)** Sequencing results confirmed the HDR R203H encoding nucleotide changes. **(C-F)** Zygotic and Maternal/Zygotic homozygous *acvr1l*$^{R203H/R203H}$embryos at 24 and 48 hpf. **(G-I)** HS and non-HS *Tg(Dr-R203Ha)*-mCherry positive homozygous *acvr1l*$^{\Delta 13bp/\Delta 13bp}$ zebrafish. **(J)** Genotyping *MZ Dr-acvr1l*$^{R203H/R203H}$ embryos. **(K)** Genotyping of rescued homozygous *Dr-acvr1l*$^{\Delta 13bp/\Delta 13bp}$ in the *Tg(Dr-R203Ha)* background after 4hpf HS (yellow asterisk =

acvr1l$^{\Delta 13bp/13bp}$). Brightfield (C, D, E, F), and merged (G-I) images are shown. Scale bars: C, E, G-I = 40μm, D, F = 40μm.

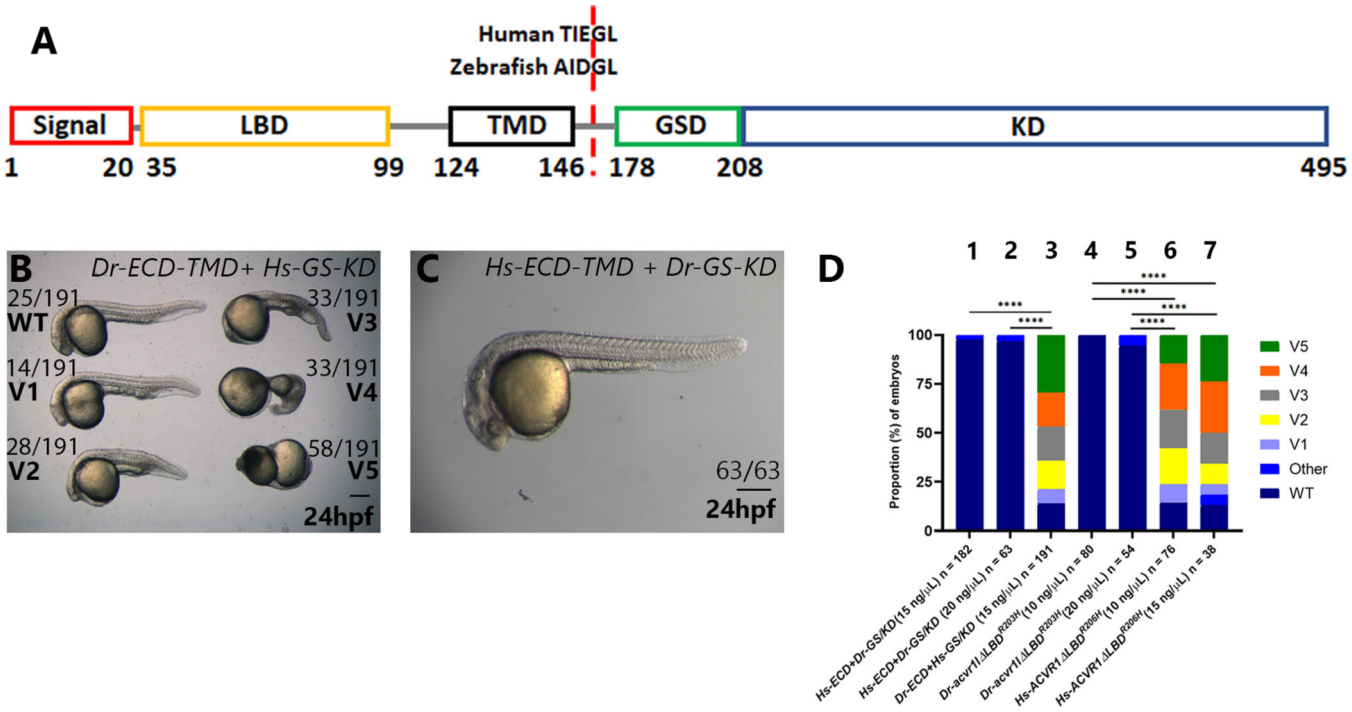

Figure 5. Chimeric receptor studies determine that Hs-ACVR1^{R206H} C-terminus directs ventralization phenotypes.

(A) Schematic of the functional domains and chimeric construct fusion location (dotted red line). Functional domains are labeled using the human amino acid sequence (Haupt et al. 2014) **(B)** *Dr-ECD-TMD + Hs-GS-KD* mRNA-injected embryos at 24. **(C)** *Hs-ECD-TMD + Dr-GS-KD* mRNA-injected embryos at 24. N values for highest injected mRNA concentration are shown in panels B-C. **(D)** Ventralization phenotypes of embryos injected with chimeric *Dr-acvr1l/Hs-ACVR1* mRNAs (Columns 1–3). The proportion of embryos with each specific phenotype (color legend displayed on the right) per group is shown **(D).** Other represents non-specific injection deformities. Concentrations and numbers of embryos injected (n =) are presented below each bar **(D)**. Each bar represents a single experiment. Significance (*) was set at $p < 0.05$. ** indicates $p < 0.01$ and **** indicates $p < 0.0001$ **(D)**. Brightfield (B, C, D) images are shown. Scale bars: B = 40μm, C-D = 40μm.

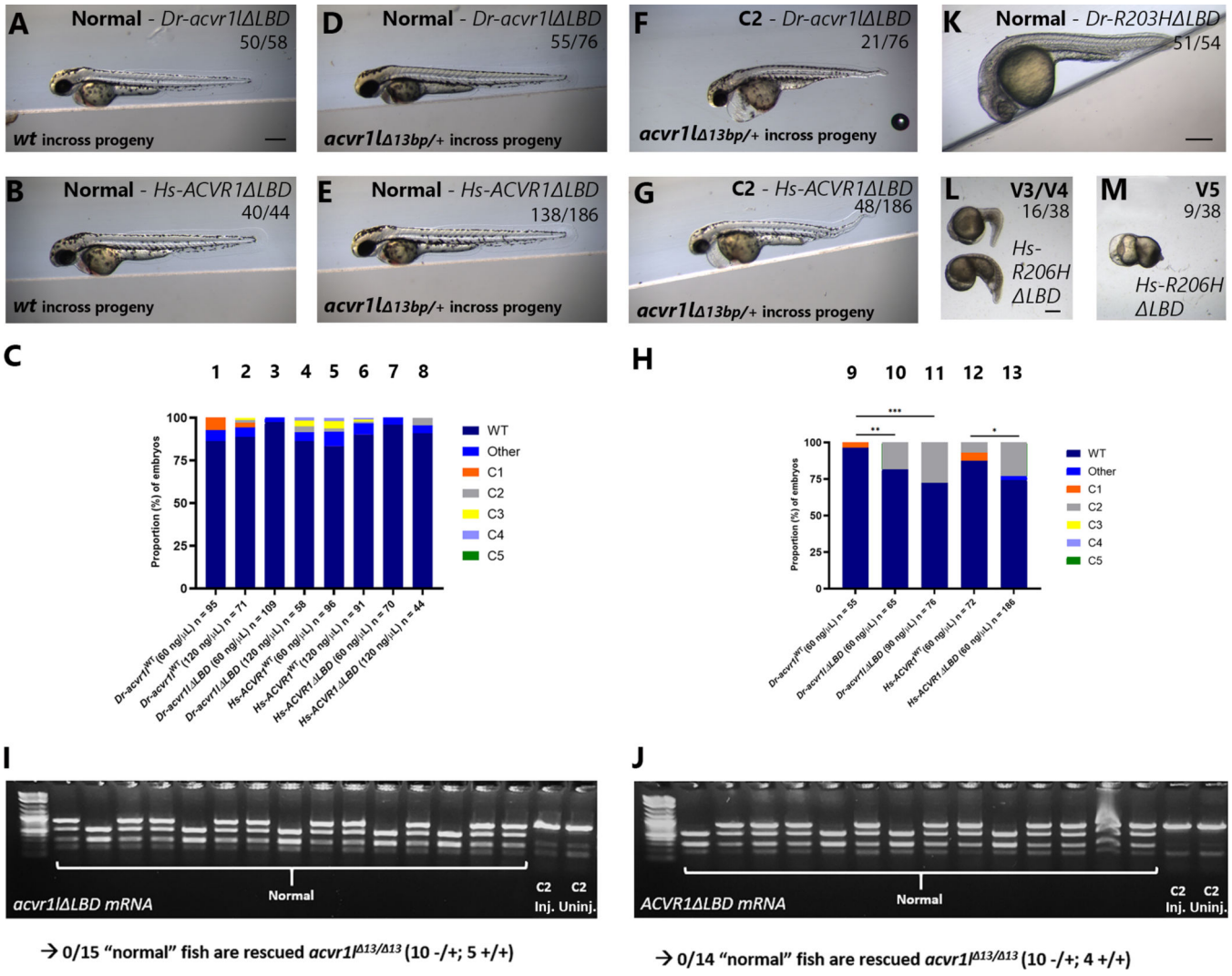

Figure 6. Hs-ACVR1^{R206H} lacking the ligand-binding domain (LBD) retained ventralization activity, while both WT Dr-Acvr1l and WT Hs-ACVR1 variants require their LBDs to function.

(A-B) Single cell injected WT Dr-*acvr1lΔLBD* or *Hs-ACVR1ΔLBD* mRNA-injected WT embryos at 48hpf. **(C)** Injection statistics of full length *Hs-ACVR1* and *Dr-acvr1l* mRNA, Dr-*acvr1lΔLBD* and *Hs-ACVR1ΔLBD* mRNA. **(D-H)** *Dr-acvr1lΔLBD* or *Hs-ACVR1ΔLBD* mRNA-injected incrossed adult heterozygous *acvr1l*$^{\Delta 13bp/+}$ progeny at 48hpf and phenotype statistics. Note that a ~25% C2-dorsalization (in grey) indicates no rescue of homozygous *acvr1l*$^{\Delta 13bp/\Delta 13bp}$ mutants. **(I-J)** Genotyping *Dr-acvr1l*ΔLBD and *Hs-ACVR1ΔLBD* mRNA-injected phenotypically normal incrossed *Dr-acvr1l*$^{\Delta 13bp/+}$ progeny. **(K-M)** *Dr-acvr1lΔLBD*^{R203H} or *Hs-ACVR1ΔLBD*^{R206H} mRNA-injected embryos at 24hpf. N values for highest injected mRNA concentration are shown in panels A-B, D-G, K-M. mRNA concentrations and number of injected embryos presented below each column **(C, H)**. The proportion of embryos of each phenotype (color legend displayed on the right) per group is shown **(C, H)**. Other represents non-specific injection deformities **(C, H)**. Concentrations and numbers of embryos injected (n) are presented below each bar. Each bar represents a single experiment. Significance (*) was set at $p < 0.05$. *** means $p < 0.001$.

(C, H). Brightfield A-B, D-G, K-M images are shown. Scale bars: A-F = 40μm, H = 40μm, I-J = 40μm.

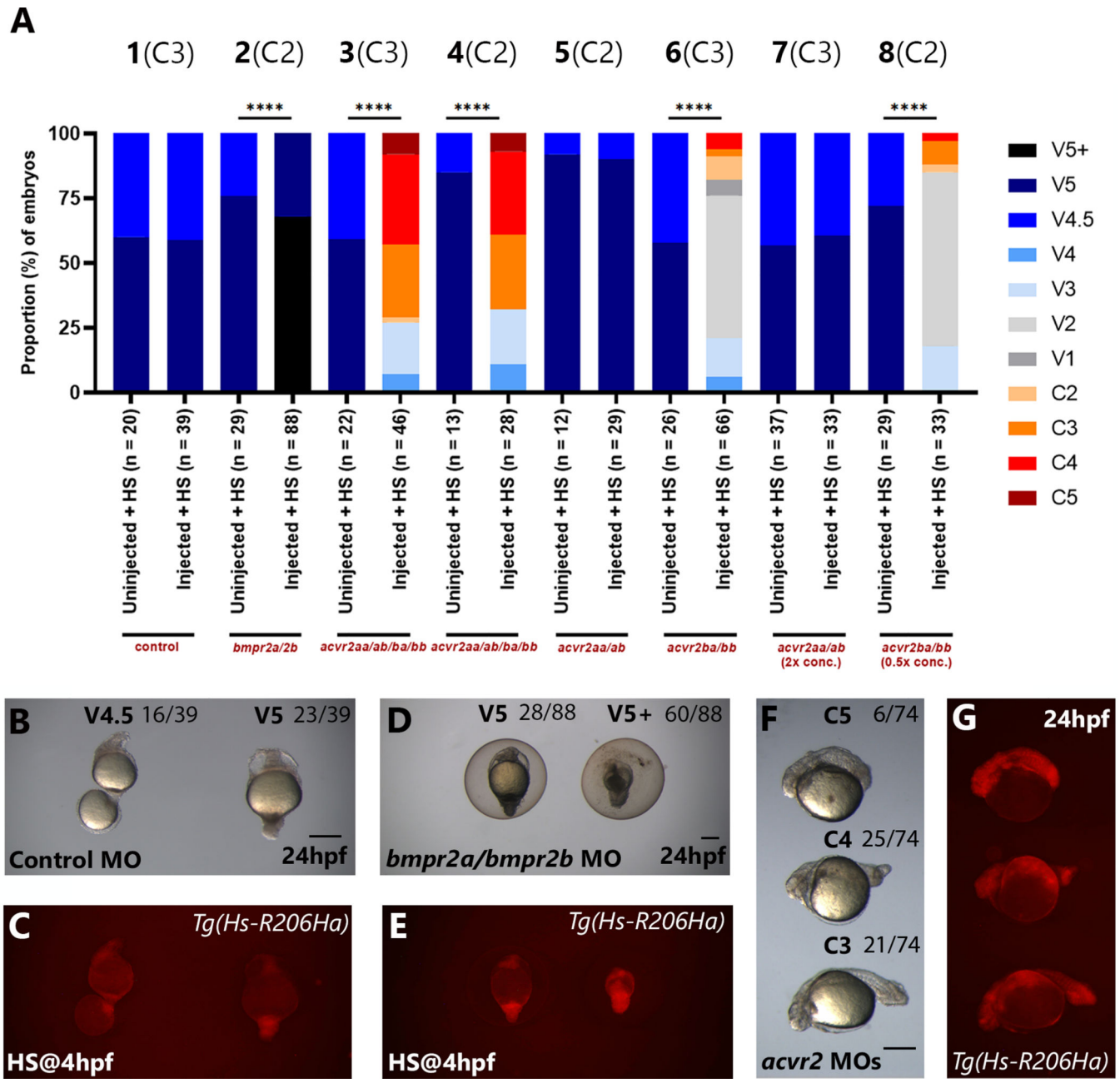

Figure 7. Acvr2a/b knockdown inhibits Hs-ACVR1^{R206H} activity in embryonic zebrafish.

(A) Bmp and Activin Type II receptor anti-sense morpholino injection into HS-*Tg(Hs-R206Ha)*-mCherry transgenic lines. **(B-G)** Ventralization/dorsalization phenotypes in 24hpf HS-*Tg(Hs-R206Ha)*-mCherry embryos following injection of control MO (**Set 1**), *bmpr2a/bmpr2b* MOs (**Set 2**), *acvr2aa/acvr2ab* MOs (**Set 5 (1x conc.), 7 (2x conc.**), *acvr2ba/acvr2bb* MOs (**Set 6 (1x conc.), 8 (0.5x conc.**), and *acvr2aa/acvr2ab/acvr2ba/acvr2bb* MOs (**Set 3, 4**). Set number, displayed at the top of the bars, refers to each pair of bars: experimental and corresponding uninjected controls. F2 *Tg(R206Ha)* incross pair (C2 = Cross 2, C3 = Cross 3) is indicated next to data set number. *acvr2aa/acvr2ab* MO 2x concentration, and *acvr2ba/acvr2bb* MO 0.5x concentration were used to control for

potential knockdown efficiencies. The proportion of embryos with each specific phenotype per group is shown (see color legend displayed on the right) **(A)**. Concentrations and numbers of embryos injected (n) are presented below each bar **(A)**. Each bar represents a single experiment. Significance (*) was set at $p < 0.05$. **** indicates $p < 0.0001$ **(A)**. Statistics from *Tg(Hs-R206Ha)*-positive embryos are included, statistics from injected, non-HS embryos are provided in Figure 7. Control MO injection plus HS yielded V4.5 and V5 ventralized embryos **(B-C),** *bmpr2aa/bmpr2ab* MO co-injection plus HS yielded V5 and V5+ ventralized embryos (**D-E**). *acvr2aa/acvr2ab/acvr2ba/acvr2bb* MO co-injection plus HS yielded mCherry-positive dorsalized embryos (**F-G**). All phenotypes were assessed at 24hpf. Brightfield (B, D, F) and mCherry (C, E, G) images are shown. Scale bars: B-C = 40μm, D-E = 40 μm, F-G = 40μm.

A

MO	Cross	Treatment	N	Classification													
				-	-	-	-	-	WT	V1	V2	V3	V4	V4.5	V5	V5+	Other
Control	3	No Inject + HS	28	-	-	-	-	-	28.60%	0%	0%	0%	0%	28.60%	42.85%	0%	0%
		Inject + No HS	41	-	-	-	-	-	100%	0%	0%	0%	0%	0%	0%	0%	0%
		Inject + HS	58	-	-	-	-	-	32.76%	0%	0%	0%	0%	27.59%	39.66%	0%	0%
Control (2x conc.)	WT	N/A	92	-	-	-	-	-	97.80%	0%	0%	0%	0%	0.00%	0.00%	0%	2%
MO	**Cross**	**Treatment**	**N**	**B5**	**B4**	**B3**	**B2**	**B1**	**WT**	**V1**	**V2**	**V3**	**V4**	**V4.5**	**V5**	**V5+**	**Other**
bmpr2a	3	No Inject + HS	28	0%	0%	0%	0%	0%	28.60%	0%	0%	0%	0%	28.60%	42.85%	0%	0%
		Inject + No HS	67	0%	0%	14.92%	26.87%	29.85%	29.85%	0%	0%	0%	0%	0%	0%	0%	0%
		Inject + HS	69	0%	0%	0%	5.80%	10.10%	15.90%	0%	0%	0%	0%	13%	44.93%	10.10%	0%
bmpr2b	3	No Inject + HS	28	0%	0%	0%	0%	0%	28.60%	0%	0%	0%	0%	28.60%	42.85%	0%	0%
		Inject + No HS	70	0%	0%	4.29%	8.57%	12.86%	74.29%	0%	0%	0%		0%	0%	0%	0%
		Inject + HS	65	0%	0%	0%	0%	3.10%	10.77%	0%	0%	0%	0%	16.90%	53.80%	15.40%	0%
bmpr2a/bmpr2b	2	No Inject + HS	37	0%	0%	0%	0%	0%	21.60%	0%	0%	0%	0%	18.90%	59.46%	0%	0%
		Inject + No HS	85	2.40%	11.80%	23.50%	25.90%	24.70%	11.76%	0%	0%	0%	0%	0%	0%	0%	0%
		Inject + HS	125	0%	0%	0%	12.80%	12.00%	4.80%	0%	0%	0%	0%	0%	22.40%	48%	0%
MO	**Cross**	**Treatment**	**N**	**C5**	**C4**	**C3**	**C2**	**C1**	**WT**	**V1**	**V2**	**V3**	**V4**	**V4.5**	**V5**	**V5+**	**Other**
acvr2aa	3	No Inject + HS	33	0%	0%	0%	0%	0%	36.40%	0%	0%	0%	0%	9.10%	54.50%	0%	0%
		Inject + No HS	58	0%	0%	0%	0%	0%	96.60%	0%	0%	0%	0%	0%	0%	0%	3.40%
		Inject + HS	66	0%	0%	0%	0%	0%	18.20%	0%	0%	0%	0%	15.20%	66.66%	0%	0%
acvr2ab	1	No Inject + HS	56	0%	0%	0%	0%	0%	25.00%	0%	0%	0%	0%	0%	75.00%	0%	0%
		Inject + No HS	44	0%	0%	0%	0%	0%	90.90%	0%	0%	0%	0%	0%	0%	0%	9.10%
		Inject + HS	59	0%	0%	0%	0%	0%	10.20%	0%	0%	0%	0%	0%	89.90%	0%	0%
acvr2aa/acvr2ab	2	No Inject + HS	19	0%	0%	0%	0%	0%	36.80%	0%	0%	0%	0%	5.30%	57.90%	0%	0%
		Inject + No HS	37	0%	0%	0%	0%	0%	89.20%	0%	0%	0%	2.70%	0%	0%	0%	8.10%
		Inject + HS	43	0%	0%	0%	0%	0%	32.60%	0%	0%	2.33%	0%	4.65%	60.50%	0%	0%
acvr2aa/acvr2ab (2x conc.)	3	No Inject + HS	47	0%	0%	0%	0%	0%	21.30%	0%	0%	0%	0%	36.40%	44.70%	0%	0%
		Inject + No HS	35	0%	0%	0%	0%	0%	94.30%	0%	0%	0%	0%	0%	0%	0%	5.70%
		Inject + HS	44	0%	0%	0%	0%	0%	25%	0%	0%	0%	0%	29.50%	45.50%	0%	0%
MO	**Cross**	**Treatment**	**N**	**C5**	**C4**	**C3**	**C2**	**C1**	**WT**	**V1**	**V2**	**V3**	**V4**	**V4.5**	**V5**	**V5+**	**Other**
Acvr2ba	1	No Inject + HS	49	0%	0%	0%	0%	0%	30.60%	0%	0%	0%	0%	8.20%	61.20%	0%	0%
		Inject + No HS	53	0%	0%	0%	35.80%	39.60%	24.50%	0%	0%	0%	0%	0%	0%	0%	0%
		Inject + HS	68	0%	0%	1.50%	5.90%	14.70%	4.40%	0%	0%	13.20%	58.80%	0%	1.50%	0%	0%
acvr2bb	3	No Inject + HS	20	0%	0%	0%	0%	0%	25%	0%	0%	0%	0%	25%	50%	0%	0%
		Inject + No HS	23	0%	0%	8.70%	4.30%	13%	73.90%	0%	0%	0%	0%	0%	0%	0%	0%
		Inject + HS	29	0%	0%	0%	3.40%	3.40%	17.20%	0%	0%	0%	58.60%	3.40%	13.80%	0%	0%
acvr2ba/acvr2bb	3	No Inject + HS (mCh+)	26	0%	0%	0%	0%	0%	0%	0%	0%	0%	0%	42.30%	57.70%	0%	0%
		Inject + No HS	57	1.80%	5.30%	7%	38.60%	38.60%	8.80%	0%	0%	0%	0%	0%	0%	0%	0%
		Inject + HS (mCh+)	66	0%	6.10%	3%	9.10%	0%	0%	6.10%	54.50%	15.20%	6.10%	0%	0%	0%	0%
		Inject + HS (mCh-)	13	7.70%	0%	0%	30.80%	23.10%	38.50%	0%	0%	0%	0%	0%	0%	0%	0%
acvr2ba/acvr2bb (0.5x conc.)	2	No Inject + HS (mCh+)	29	0%	0%	0%	0%	0%	0%	0%	0%	0%	0%	26.70%	73.30%	0%	0%
		Inject + No HS	23	0%	13%	34.80%	21.70%	21.70%	8.70%	0%	0%	0%	0%	0%	0%	0%	0%
		Inject + HS (mCh+)	33	0%	3%	9.10%	3%	0%	0%	0%	66.70%	18.20%	0%	0%	0%	0%	0%
		Inject + HS (mCh-)	10	0%	0%	10%	30%	30%	30%	0%	0%	0%	0%	0%	0%	0%	0%
MO	**Cross**	**Treatment**	**N**	**C5**	**C4**	**C3**	**C2**	**C1**	**WT**	**V1**	**V2**	**V3**	**V4**	**V4.5**	**V5**	**V5+**	**Other**
acvr2aa/acvr2ab *acvr2ba/acvr2bb*	2	No Inject + HS (mCh+)	13	0%	0%	0%	0%	0%	0%	0%	0%	0%	0%	15.40%	84.60%	0%	0%
		Inject + No HS	26	0%	30.80%	34.60%	7.70%	11.50%	15.40%	0%	0%	0%	0%	0%	0%	0%	0%
		Inject + HS (mCh+)	28	7.14%	32.10%	28.60%	0%	0%	0%	0%	0%	21.40%	10.70%	0%	0%	0%	0%
		Inject + HS (mCh-)	13	0%	30.80%	30.80%	15.40%	15.40%	7.70%	0%	0%	0%	0%	0%	0%	0%	0%
acvr2aa/acvr2ab *acvr2ba/acvr2bb*	3	No Inject + HS (mCh+)	22	0%	0%	0%	0%	0%	0%	0%	0%	0%	0%	40.90%	59.10%	0%	0%
		Inject + No HS	27	0%	29.63%	37%	11.11%	11.11%	11.11%	0%	0%	0%	0%	0%	0%	0%	0%
		Inject + HS (mCh+)	46	8.70%	34.80%	28.30%	2.20%	0%	0%	0%	0%	19.60%	6.50%	0%	0%	0%	0%
		Inject + HS (mCh-)	9	0%	22.22%	44.44%	33.33%	0%	0%	0%	0%	0%	0%	0%	0%	0%	0%

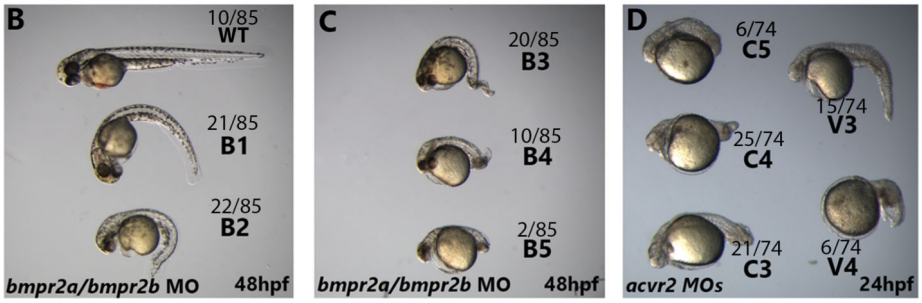

Figure 8. Acvr2a/b knockdown inhibited Hs-ACVR1^{R206H} activity in early embryonic zebrafish.

(A) Summarized results of Type II receptor anti-sense MO injections into single cell stage *Tg(Hs-R206Ha)* embryos. **(B-C)** Dorsalization spectrum (B1-B5) of *bmpr2a/bmpr2b* anti-sense MO injected and HS single cell stage *Tg(Hs-R206Ha)* embryos at 48hpf. **(D)** 24hpf dorsalization and ventralization phenotypes of single cell stage *acvr2* MO-injected and HS embryos. Unless noted, mCherry-positive and mCherrynegative embryos were totaled together. *Tg(Hs-R206Ha)*-positive embryos, verified by mCherry fluorescence, are indicated in red text **(A)**. Co-injected *acvr2aa/acvr2ab/acvr2ba/acvr2bb* or *acvr2ba/acvr2bb* MOs

yielded mCherry-positive dorsalized embryos, and therefore were totaled independently from mCherry-negative dorsalized embryos (Labeled HS + Inject (mCh+)). No inject + HS = No MO injection plus heat-shock, Inject + No HS = MO injection without Heat-shock, Inject + HS = MO injection plus heat-shock. *Tg(Hs-R206Ha)* incross ID indicated in third column. Number of embryos (N) indicated in fourth column **(A)**. “Other” phenotype represents injection defects **(A)**. Phenotypic stats taken at 24hpf. Brightfield (B-D) images are shown.

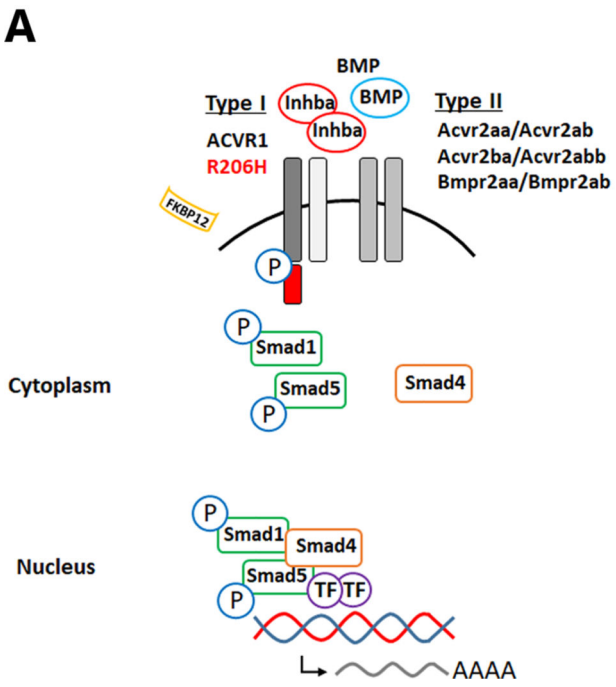

B

Type II receptor morpholino summary

Morpholino	R206H signaling (ventralization severity)
bmpr2aa/bmpr2ab	Increased
acvr2aa/acvr2ab	No change
acvr2ba/acvr2bb	Decreased
acvr2aa/acvr2ab *acvr2ba/acvr2bb*	Decreased

Figure 9. Summary of Hs-R206H signaling pathway and type II receptor MO injection results.

Hs-ACVR1/Type I receptor heterodimers can oligomerize with ACVR2A (Acvr2aa/Acvr2ab), ACVR2B (Acvr2ba/Acvr2bb), and BMPR2A (Bmpr2aa/Bmpr2ab). We predicted that targeted knockdown of type II signaling partners of Hs-ACVR1^{R206H} via MO injections would result in decreased signaling, and ventralization severity, in *HS-Tg(Hs-R206Ha)* embryos. (B) Summary of results from MO injections on ACVR1^{R206H} signaling and ventralization severity *HS-Tg(HS-R206Ha)* embryos.